# A massive cluster of Red Supergiants at the base of the Scutum-Crux arm

Ben Davies[1], Don F. Figer[1], Rolf-Peter Kudritzki[2], John MacKenty[3], Francisco Najarro[4] and Artemio Herrero[5]

[1] *Chester F. Carlson Center for Imaging Science, Rochester Institute of Technology, 54 Lomb Memorial Drive, Rochester NY, 14623, USA*

[2] *Institute for Astronomy, University of Hawaii, 2680 Woodlawn Drive, Honolulu, HI, 96822, USA*

[3] *Space Telescope Science Institute, 3700 San Martin Drive, Baltimore, MD, 21218, USA*

[4] *Instituto de Estructura de la Materia, Consejo Superior de Investigaciones Científicas, Calle Serrano 121, 28006 Madrid, Spain.*

[5] *Instituto de Astrofsica de Canarias, Via Làctea S/N, E-38200 La Laguna, Tenerife, Spain*

## ABSTRACT

We report on the unprecedented Red Supergiant (RSG) population of a massive young cluster, located at the base of the Scutum-Crux Galactic arm. We identify candidate cluster RSGs based on *2MASS* photometry and medium resolution spectroscopy. With follow-up high-resolution spectroscopy, we use CO-bandhead equivalent width and high-precision radial velocity measurements to identify a core grouping of 26 physically-associated RSGs – the largest such cluster known to-date. Using the stars' velocity dispersion, and their inferred luminosities in conjuction with evolutionary models, we argue that the cluster has an initial mass of $\sim$40,000$M_\odot$, and is therefore among the most massive in the galaxy. Further, the cluster is only a few hundred parsecs away from the cluster of 14 RSGs recently reported by Figer et al (2006). These two RSG clusters represent 20% of all known RSGs in the Galaxy, and now offer the unique opportunity to study the pre-supernova evolution of massive stars, and the Blue- to Red-Supergiant ratio at uniform metallicity. We use GLIMPSE, MIPSGAL and MAGPIS survey data to identify several objects in the field of the larger cluster which seem to be indicative of recent region-wide starburst activity at the point where the Scutum-Crux arm intercepts the Galactic bulge. Future abundance studies of these clusters will therefore permit the study of the chemical evolution and metallicity gradient of the Galaxy in the region where the disk meets the bulge.

*Subject headings:* open clusters & associations, supergiants, stars:evolution, stars:late-type

## 1. Introduction

Massive stars play a pivotal role in the evolution of their host galaxies. As main-sequence O stars, they emit copious amounts of ionizing UV radiation. Their post-MS evolution is characterized by brief but extreme mass-losing episodes, such as the Red Supergiant (RSG), Luminous Blue Variable (LBV) and Wolf-Rayet (WR) phases, during which they inject the interstellar medium (ISM) with mechanical energy and chemically-processed material. When they end their lives as core-collapse supernovae (SNe), they inject the ISM with heavy elements and drive shocks into their surroundings, strongly influencing subsequent local star-formation.

The stellar end state, i.e. neutron star, black-hole, or complete disruption, depends on the terminal mass of the star (Heger et al. 2003). Additionally, the appearance of the SN explosion is thought to be linked to the progenitor. The hydrogen-poor Type Ib+c SN are thought to have WR progenitors, while the progenitors of many of the H-rich Type II-P have been identified as RSGs from archival *HST* images (Van Dyk et al. 2003; Smartt et al. 2004; Maund et al. 2004). However, the most clear-cut case of a Type II-P progenitor remains SN1987A, which was a Blue Supergiant (BSG) (Sonneborn et al. 1987).

Predicting the evolution of massive stars from post-main sequence to the end of their lives is notoriously problematic. It is driven by the star's mass-loss behaviour, which in turn is strongly dependent on factors such as metallicity and rotation which are poorly constrained (see review of Kudritzki & Puls 2000). Meanwhile, empirical studies of massive stellar evolution are hampered by low-number statistics, due to the steepness of the Initial Mass Function (IMF), the short lifetimes of the stars, and the obcurring effect of the gas and dust in the Galactic plane.

Galactic young massive clusters provide us with the ideal natural laboratories in which to study massive stellar evolution. Such objects provide a coeval sample of massive stars under the constraint of uniform metallicity, whilst being close enough to resolve the individual stars. Unfortunately, such objects are rare. Until recently, only Westerlund 1 (Wd 1, Clark et al. 2005), the Arches Cluster (Figer et al. 2002), the Quintuplet Cluster (Figer et al. 1999), and the Galactic Centre (GC) cluster (Figer et al. 2004) were known to be massive enough and young enough to harbour statistically-significant numbers of massive stars. Ages of these clusters range from ∼3Myr (Arches) to ∼5Myr (Wd 1). Hence, while they are both

young and massive enough to contain large numbers of O stars and WRs, they are *too* young to have similar numbers of RSGs, which are expected after $\sim$6Myr.

Using catalogues of Galactic Plane cluster candidates (Bica et al. 2003a,b; Dutra et al. 2003), Figer et al. (2006, hereafter FMR06) made the discovery of an unprecedented cluster of 14 RSGs at a Galactic longitude of $l = 25°$, hereafter known as RSGC1. At the time of discovery this object contained by far the greatest number of RSGs of all known Galactic clusters, a record previously held by NGC 7419 with 5 (Caron et al. 2003).

RSGC1 is located at the base of the Scutum-Crux arm, close to where it meets the Galactic bulge. It is separated by $\sim$1° from another reddened cluster, Stephenson 2. In the discovery paper, Stephenson (1990) speculated that the cluster may harbour several RSGs, possibly up to 10, based on the brightness of the stars in the $I$ band. The cluster was also studied by Nakaya et al. (2001) and Ortolani et al. (2002), who estimated distances of 1.5kpc/5.9kpc, and ages of 50Myr/20Myr respectively, from optical and infrared photometry.

Here, we present low- and high-resolution spectroscopy of over 40 red stars in this cluster, and combine this with *2MASS*, *MSX* and *GLIMPSE* photometry. We show from high-precision radial velocity measurements and IR photometry that the cluster, hereafter known as RSGC2, is host to 26 RSGs, by far the largest known population in the Galaxy. We use this velocity information, in conjuction with the stars' spectra and stellar evolution models to better constrain the distance and age of the cluster.

Between them RSGC1 and 2 are host to $\sim$20% of all known RSGs in the Galaxy, and now offer us the opportunity to study a coeval sample of Type II-P SN progenitors, as well as the BSG/RSG ratio important in constraining stellar evolutionary models, at uniform metallicity. Further, the location of the clusters within the Galaxy will allow future metallicity studies to probe the apparent chemical discontinuity observed to exist between the Galactic disk and bulge (see e.g. Ramírez et al. 2000; Smartt et al. 2001; Najarro et al. 2004).

We begin in Sect. 2 with a description of our observations, including target selection, data reduction and analysis techniques. We present the results of the data analysis in Sect. 3, and argue which of the stars observed are members of the cluster. In Sect. 4 we estimate the cluster age and mass, before discussing the two remarkable Scutum-Crux RSGCs in the context of of other massive Galactic clusters, and their significance in the study of various aspects of stellar/galactic evolution.

## 2.   Observations & data reduction

### 2.1.   Target selection & strategy

For a coeval population of stars, RSGs are typically $\sim$4 mags brighter in the $K$-band than any other stars in the cluster. Therefore, in order to identify potential RSGs, we compliled a list of candidate stars within an 7′ radius of the cluster centre (as defined by Stephenson 1990) based on their $K_S$-band magnitudes in the Two-Micron All Sky Survey (*2MASS*) point-source catalogue (Cutri et al. 2003).

A key spectral diagnostic for late-type stars is the CO bandhead feature at $2.295\mu$m. As shown in FMR06, the feature is evident in spectral-type G and later, and is extremely prominant in M-type stars. Further, the feature is stronger in supergiants than giants and dwarfs. To identify those stars with CO absorption, we observed the brightest 50 stars in our target list, as well as others, with *IRMOS* – the Infra-Red Multi-Object Spectrograph (MacKenty et al. 2003) – at the KPNO-4m during April 2006.

It is likely that this CO sub-sample of stars is contaminated by foreground/unrelated M dwarfs and giants. To determine which of our sample are physically related, we obtained follow-up high-resolution spectroscopic data of the CO feature to measure high-precision radial velocities of the stars. These data were taken with *NIRSPEC*, the cross-dispersed echelle spectrograph at the Keck II telescope (McLean et al. 1998), during two observing runs in May and August 2006. In total we observed all but one of the brightest 33 stars, as well as 11 others. As will be shown in Sect. 3, the fainter stars of the sample are more likely to be foreground objects and not supergiants, therefore the few stars we missed will not have a significant impact on our conclusions.

Table 1 lists the brightest 72 stars within a 7′ radius of the cluster centre, together with their *2MASS* photometry and the dates observed. The stars are indexed in order of their $K_S$-band magnitude; also listed are any identification in Stephenson (1990) and Nakaya et al. (2001). A *2MASS* $K_S$-band image of RSGC2 is shown in Fig. 1a, and Fig. 1b shows a finding chart for the stars. Both the K-band image and the finding chart are centered on the approximate center of the cluster, $18^h39'20.4''$, $-6°01'41''$, epoch 2000 (Star 5 in S90, Star 14 in this paper).

### 2.2.   *IRMOS* observations

The Infra-red Multi-Object Spectrograph (*IRMOS*, MacKenty et al. 2003), uses a micro-mirror array of $\sim10^6$ elements. Synthetic 'slits' can be defined by switching selected mirrors of
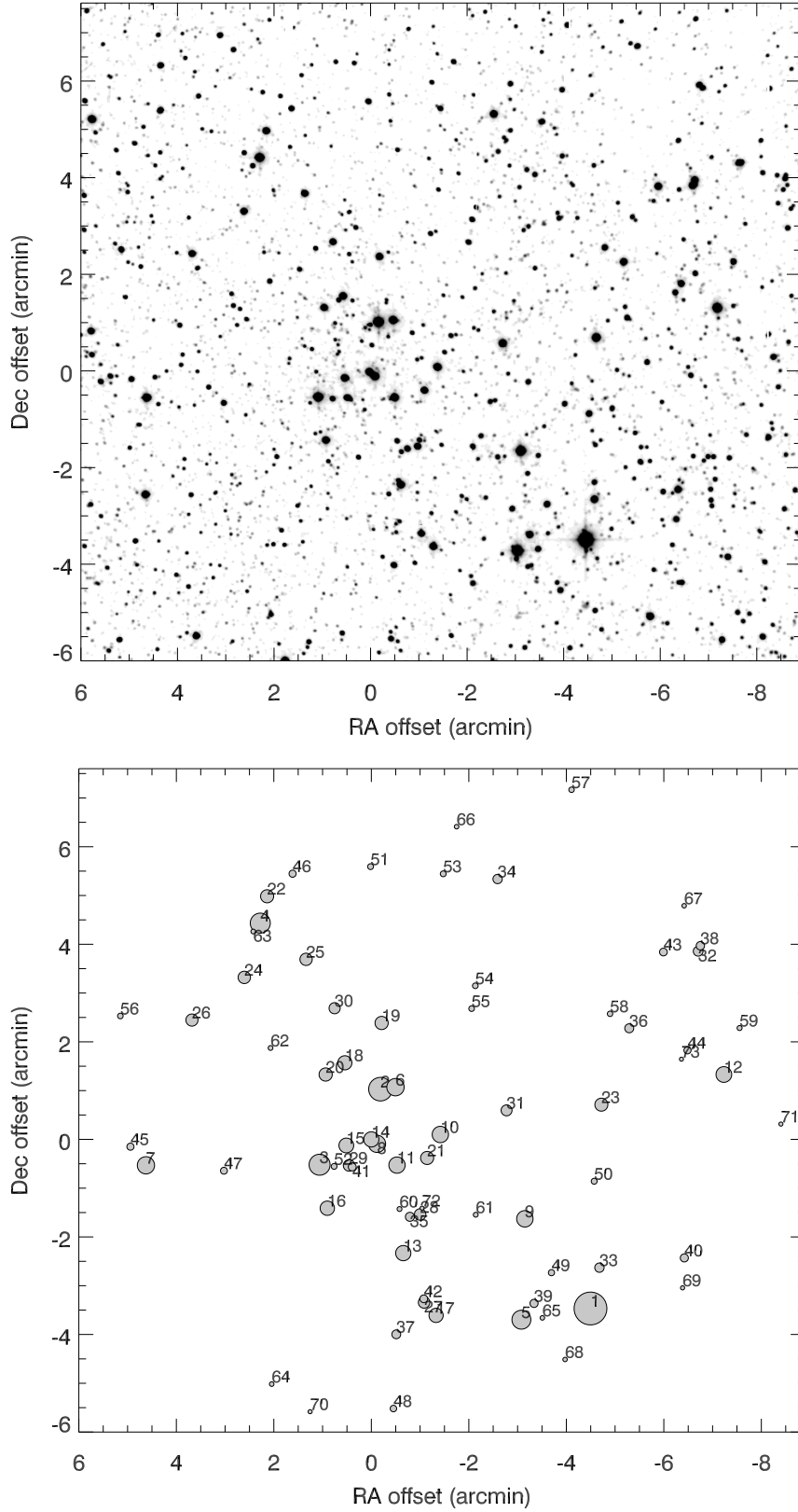
**Fig. 1.**—: 2MASS K-band image of RSGC2 (*upper*), and finding chart (*lower*). Coordinates are centered on 18 39 20.4, -6 01 41 (2000), following Stephenson (1990). The sizes of the plotting symbols scale linearly with K-band magnitude.

**Table 1::** Observational data for the brightest stars in the *2MASS* point-source catalogue within 7′ of the cluster center. Star are indexed according to their $K_S$-band magnitudes (column 1). Columns 2 and 3 denote identifications in the previous studies of Stephenson (1990) and Nakaya et al. (2001). Columns 4 and 5 list the J2000 coordinates of each star, and the *2MASS* photometry is listed in columns 6-8. The *NIRSPEC* observation date is listed in the final column. Note that Star 32b is not resolved in *2MASS* due to its proximity to Star 32.

| ID | S90 | N01 | RA | Dec | J | H | $K_s$ | Obs Date | |
|----|-----|-----|-----|-----|---|---|-------|----------|---|
| | | | | (J2000) | | | | *NIRSPEC* | *IRMOS* |
| 1 | | | 18 39 02.4 | -06 05 10.6 | 7.15 | 4.698 | 2.900 | 08/12/06 | 04/17/06 |
| 2 | 2 | | 18 39 19.6 | -06 00 40.8 | 6.899 | 5.045 | 4.117 | 05/05/06 | |
| 3 | 10 | | 18 39 24.6 | -06 02 13.8 | 7.273 | 5.458 | 4.499 | 05/05/06 | |
| 4 | | | 18 39 29.5 | -05 57 16.6 | 7.906 | 5.705 | 4.647 | 08/12/06 | 04/18/06 |
| 5 | | | 18 39 08.1 | -06 05 24.4 | 8.532 | 6.054 | 4.822 | 08/12/06 | 04/17/06 |
| 6 | 1 | | 18 39 18.4 | -06 00 38.4 | 7.717 | 5.919 | 5.062 | 05/05/06 | |
| 7 | | | 18 39 38.9 | -06 02 14.5 | 7.585 | 5.867 | 5.090 | 08/12/06 | 04/20/06 |
| 8 | 4 | | 18 39 19.9 | -06 01 48.1 | 7.817 | 6.015 | 5.106 | 05/05/06 | |
| 9 | | | 18 39 06.8 | -06 03 20.3 | 8.569 | 6.308 | 5.233 | 08/12/06 | 04/17/06 |
| 10 | | 1102 | 18 39 14.7 | -06 01 36.6 | 8.218 | 6.214 | 5.244 | 05/05/06 | |
| 11 | | 1180 | 18 39 18.3 | -06 02 14.3 | 8.354 | 6.207 | 5.256 | 05/05/06 | |
| 12 | | | 18 38 51.4 | -06 00 22.8 | 7.221 | 5.943 | 5.354 | - | |
| 13 | | 1230 | 18 39 17.7 | -06 04 02.5 | 8.421 | 6.387 | 5.439 | 08/12/06 | 04/17/06 |
| 14 | 5 | | 18 39 20.4 | -06 01 42.6 | 8.222 | 6.355 | 5.443 | 05/05/06 | |
| 15 | 6 | | 18 39 22.4 | -06 01 50.1 | 8.129 | 6.346 | 5.513 | 05/05/06 | |
| 16 | 8 | | 18 39 24.0 | -06 03 07.3 | 8.235 | 6.444 | 5.597 | 05/05/06 | |
| 17 | | | 18 39 15.1 | -06 05 19.1 | 8.709 | 6.613 | 5.619 | 08/12/06 | 04/17/06 |
| 18 | 7 | | 18 39 22.5 | -06 00 08.4 | 8.179 | 6.451 | 5.632 | 08/12/06 | |
| 19 | 3 | | 18 39 19.5 | -05 59 19.4 | 8.282 | 6.584 | 5.801 | 08/12/06 | |
| 20 | 9 | | 18 39 24.1 | -06 00 22.8 | 8.426 | 6.656 | 5.805 | 08/12/06 | |
| 21 | | 598 | 18 39 15.8 | -06 02 05.5 | 9.115 | 6.925 | 5.824 | 05/05/06 | |
| 22 | | | 18 39 28.9 | -05 56 43.6 | 9.142 | 7.071 | 5.825 | 08/12/06 | 04/18/06 |
| 23 | | | 18 39 01.5 | -06 00 59.9 | 10.088 | 7.219 | 5.840 | 08/13/06 | 04/20/06 |
| 24 | | | 18 39 30.8 | -05 58 23.3 | 7.356 | 6.368 | 5.960 | 08/12/06 | 04/17/06 |
| 25 | | | 18 39 25.7 | -05 58 01.1 | 8.911 | 6.965 | 5.975 | 08/12/06 | 04/17/06 |
| 26 | | | 18 39 35.1 | -05 59 15.8 | 8.676 | 6.902 | 6.003 | 08/12/06 | 04/17/06 |
| 27 | | | 18 39 16.0 | -06 05 03.2 | 9.058 | 7.055 | 6.129 | 08/12/06 | 04/17/06 |
| 28 | | | 18 39 16.4 | -06 03 15.0 | 7.626 | 6.589 | 6.132 | 08/12/06 | 04/17/06 |
| 29 | | | 18 39 22.2 | -06 02 14.7 | 8.608 | 6.877 | 6.146 | 05/05/06 | |
| 30 | | | 18 39 23.4 | -05 59 01.3 | 8.711 | 6.956 | 6.200 | 08/12/06 | |
| 31 | | 978 | 18 39 09.3 | -06 01 06.9 | 9.373 | 7.232 | 6.244 | 08/13/06 | 04/20/06 |
| 32 | | | 18 38 53.5 | -05 57 51.2 | 9.676 | 7.571 | 6.490 | 08/13/06 | |
| 32b | | | 18 38 52.8 | -05 57 40.0 | - | - | - | 08/13/06 | |

**Table 1::** Cont.

| ID | S90 | N01 | RA | Dec | J | H | $K_s$ | Obs Date | |
|----|-----|-----|-----|-----|-----|-----|-----|-----|-----|
| | | | (J2000) | | | | | *NIRSPEC* | *IRMOS* |
| 33 | | | 18 39 01.6 | -06 04 20.4 | 10.359 | 7.861 | 6.581 | 08/12/06 | 04/17/06 |
| 34 | | | 18 39 10.0 | -05 56 22.4 | 9.691 | 7.579 | 6.585 | - | |
| 35 | | | 18 39 17.2 | -06 03 17.9 | 8.878 | 7.291 | 6.651 | 08/12/06 | 04/17/06 |
| 36 | | | 18 38 59.2 | -05 59 26.0 | 11.133 | 8.142 | 6.655 | 08/13/06 | |
| 37 | | | 18 39 18.3 | -06 05 42.4 | 10.177 | 7.843 | 6.693 | - | |
| 38 | | | 18 38 53.4 | -05 57 44.4 | 8.572 | 7.324 | 6.794 | 08/13/06 | |
| 39 | | | 18 39 07.0 | -06 05 04.4 | 9.695 | 7.764 | 6.846 | - | 04/17/06 |
| 40 | | | 18 38 54.7 | -06 04 08.4 | 10.240 | 7.929 | 6.862 | - | |
| 41 | | | 18 39 21.9 | -06 02 16.5 | 9.452 | 7.781 | 6.904 | - | |
| 42 | | | 18 39 16.1 | -06 04 58.7 | 12.443 | 8.872 | 6.936 | - | |
| 43 | | | 18 38 56.4 | -05 57 52.2 | 10.621 | 8.118 | 6.947 | 08/13/06 | |
| 44 | | | 18 38 54.4 | -05 59 53.1 | 8.325 | 7.359 | 7.077 | - | |
| 45 | | | 18 39 40.1 | -06 01 51.6 | 9.749 | 7.981 | 7.085 | - | 04/20/06 |
| 46 | | | 18 39 26.8 | -05 56 15.8 | 9.994 | 8.203 | 7.086 | 08/12/06 | 04/18/06 |
| 47 | | | 18 39 32.5 | -06 02 21.2 | 9.102 | 7.741 | 7.144 | - | 04/20/06 |
| 48 | | | 18 39 18.6 | -06 07 13.7 | 11.873 | 8.841 | 7.242 | - | |
| 49 | | | 18 39 05.6 | -06 04 26.6 | 14.228 | 9.919 | 7.324 | 08/12/06 | 04/17/06 |
| 50 | | | 18 39 02.1 | -06 02 34.1 | 9.676 | 8.204 | 7.394 | - | |
| 51 | | | 18 39 20.4 | -05 56 07.1 | 12.978 | 9.400 | 7.406 | - | |
| 52 | | | 18 39 23.4 | -06 02 15.9 | 11.274 | 8.763 | 7.419 | 05/05/06 | |
| 53 | | | 18 39 14.5 | -05 56 15.9 | 9.463 | 8.011 | 7.420 | - | |
| 54 | | | 18 39 11.8 | -05 58 33.7 | 9.746 | 8.169 | 7.462 | - | |
| 55 | | | 18 39 12.1 | -05 59 01.8 | 10.419 | 8.396 | 7.471 | - | |
| 56 | | | 18 39 41.0 | -05 59 10.8 | 10.521 | 8.399 | 7.479 | - | |
| 57 | | | 18 39 03.9 | -05 54 32.5 | 12.332 | 9.240 | 7.518 | - | |
| 58 | | | 18 39 00.8 | -05 59 08.2 | 12.261 | 9.086 | 7.522 | 08/13/06 | |
| 59 | | | 18 38 50.1 | -05 59 25.6 | 9.285 | 8.109 | 7.635 | - | |
| 60 | | | 18 39 18.1 | -06 03 08.3 | 10.756 | 8.721 | 7.679 | 08/12/06 | |
| 61 | | | 18 39 11.8 | -06 03 15.3 | 10.972 | 8.721 | 7.685 | 08/12/06 | 04/17/06 |
| 62 | | | 18 39 28.6 | -05 59 50.2 | 11.147 | 8.934 | 7.692 | - | |
| 63 | | | 18 39 30.1 | -05 57 26.9 | 10.799 | 8.732 | 7.717 | - | 04/18/06 |
| 64 | | | 18 39 28.5 | -06 06 43.6 | 9.246 | 8.148 | 7.749 | - | |
| 65 | | | 18 39 06.3 | -06 05 22.2 | 12.850 | 9.520 | 7.767 | - | 04/17/06 |

**Table 1::** Cont.

| ID | S90 | N01 | RA | Dec | J | H | $K_s$ | Obs Date | |
|----|-----|-----|-----|-----|---|---|-------|----------|---|
| | | | | (J2000) | | | | *NIRSPEC* | *IRMOS* |
| 66 | | | 18 39 13.4 | -05 55 18.0 | 10.927 | 8.787 | 7.768 | - | |
| 67 | | | 18 38 54.7 | -05 56 55.2 | 13.924 | 9.788 | 7.791 | - | |
| 68 | | | 18 39 04.5 | -06 06 13.4 | 11.298 | 8.904 | 7.806 | - | |
| 69 | | | 18 38 54.8 | -06 04 45.3 | 13.447 | 9.676 | 7.886 | - | |
| 70 | | | 18 39 25.4 | -06 07 17.6 | 9.542 | 8.370 | 7.896 | - | |
| 71 | | | 18 38 46.8 | -06 01 23.8 | 12.651 | 9.446 | 7.903 | - | |
| 72 | | | 18 39 16.2 | -06 03 07.2 | 12.196 | 9.506 | 7.920 | 08/12/06 | |

the array into the 'on' position. We split the cluster up into sub-fields, and using pre-imaging data defined a series of slits at the positions of stars in the current field. We interweaved science frames with 'all-off' frames, to make an accurate measure of the dark current and instrumental background, and took flat-field observations for each MOS configuration with a continuum lamp. We observed the A star HD 44612 as a telluric standard.

### 2.2.1.   IRMOS Data reduction

For each science frame, we subtracted the corresponding dark frame and extracted sub-frames containing each of the spectra. Each sub-frame was divided through by its associated flat-field in the continuum-lamp exposures, to correct for pixel-to-pixel variations in sensitivity. Sky-subtraction was done by interpolation of the regions either side of the star, and the spectra were optimally-extracted by weighting the pixels according to the strength of the signal above the sky background. Wavelength calibration was done using the sky emission lines and telluric absorption features. The Br $\gamma$ absorption was removed from the telluric standard via linear interpolation of the continuum, and the resulting spectrum used to correct for telluric absorption.

### 2.3.   *NIRSPEC* observations

We used the instrument in high-resolution mode, with the NIRSPEC-7 filter, in conjunction with the $0.576'' \times 24''$ slit. The dispersion angle was set to $62.53°$, with cross-dispersion angle set to $35.53°$. This gave us a spectral resolution of ~17,000 in the wavelength range of 1.9-2.4$\mu$m.

We integrated on each star for 20s in each of two nod-positions along the slit. In addition to the cluster stars, we also observed HD 171305, a B0 V star, as a telluric standard on each night. Flat-fields were taken with a continuum lamp. For wavelength calibration purposes, arc frames were taken with Ar, Ne, Xe and Kr lamps to provide as many template lines as possible in the narrow wavelength range of each spectral order. To fully sample the wavelength regions between the spectral lines, we also observed the continuum lamp through an etalon filter.

### 2.3.1. NIRSPEC Data reduction

Removal of sky emission, dark current and bias offset was done by subtracting nod-pairs, and images were flat-fielded with the continuum-lamp exposures. Correction for the warping of the order images on the detector (*rectification*) was done following the method described in detail by Figer et al. (2003). An outline of the method is presented below.

The 2-D transformation matrix which corrects for the warping of the orders is known as the *rectification matrix*, and must compensate for the warping in both the spatial and spectral directions. Correction in the spatial direction was found from polynomial fitting to the two offset star traces in a nod-pair. In the spectral direction, we first found an initial wavelength solution by fitting a first-order polynomial to the arc lines in each order. This solution was then applied to the etalon frames, giving an estimate of the etalon-line wavelengths, and hence of the separation of the etalon plates. The wavelengths of the etalon lines were then recalculated, assuming that the wavelengths are determined by the equation $\lambda_n = t/2n$, where $t$ is the plate separation and $\lambda_n$ is the wavelength of the $n$th order. These recalculated wavelengths were fitted with a 3rd-order polynomial to make a secondary estimate of the rectification matrix. This solution was applied to the arc frame, and the residuals between the measured and rest-frame wavelengths of the arc lines used to fine-tune the etalon-plate thickness.

After rectifying the data, spectra were extracted by summing the pixels across the star trace in each channel. Relative shifts in wavelength of $\lesssim 4 \, \mathrm{km \, s^{-1}}$, due to the star not being in the exact centre of the slit, were corrected for by cross-correlating with a reference spectrum around the atmospheric $CO_2$ feature beginning at $\sim 1.95 \mu$m. The mean shift was taken to be the slit-centre, and the spectra of all orders shifted accordingly.

The final absolute wavelength solution, applied to all *NIRSPEC* data, was accurate to better than $\pm 4 \, \mathrm{km \, s^{-1}}$ across all orders, based on the residuals of the arc line wavelengths. The *internal* wavelength error between spectra, measured from the 1.95$\mu$m $CO_2$ feature, was

less than $\pm 1 \, \mathrm{km \, s^{-1}}$.

Cosmic ray hits and bad pixels were corrected for by taking the ratio of individual exposures of the same object, and identifiying pixels outside $5\sigma$ of the residual spectrum. Cosmic hits were replaced with the median value of the three neighbouring pixels either side. We removed the H and He I absorption features of the telluric standard via linear interpolation either side of the line. The atmospheric absorption features in the science frames were then removed by dividing through by the telluric standard. Finally, the spectra were normalised by dividing through by the median continuum value. From featureless continuum regions in the final spectra, we estimate the signal-to-noise to be better than 100 for all spectra.

## 2.4. Data analysis

### 2.4.1. Temperature estimation

We estimate the temperatures and spectral types of the stars empirically from the equivalent width of the CO bandhead feature, $EW_{\mathrm{CO}}$. We calibrate this method with template spectra of Red Giants and Red Supergiants taken from Kleinmann & Hall (1986), Wallace & Hinkle (1996b) and Wallace & Hinkle (1997). To do this, we define a measurement region of 2.294-2.304$\mu$m in the rest frame. The definition of a robust local continuum region is problematic, due to the dense molecular and atomic absorption lines in this region of the spectrum. Our continuum measurements were made from the median-average of the 2.288–2.293$\mu$m region. We estimated an uncertainty on the $EW_{\mathrm{CO}}$ measurement by making small adjustments in the definition of the continuum region and checking the repeatibility. We found that the measurements were stable to around 1Å, or $\sim 5\%$.

Figure 2 shows the correlation between spectral types of the template stars and $EW_{\mathrm{CO}}$ as measured across the predefined wavelength range. It can be seen that the relationship between the two is approximately linear, while for a given spectral type supergiants tend to show stronger CO absorption than giants. We determined the spectral types of those stars classified as supergiants from the linear fit to the literature data shown in Fig. 2. For the template giants the rms scatter on the fit is $\pm 1$ subtype, while the scatter is larger for the template supergiants ($\pm 2$ subtypes). This is the uncertainty we adopt throughout the rest of this paper. In converting spectral type to effective temperature, we use the temperature scale recently rederived by Levesque et al. (2005).
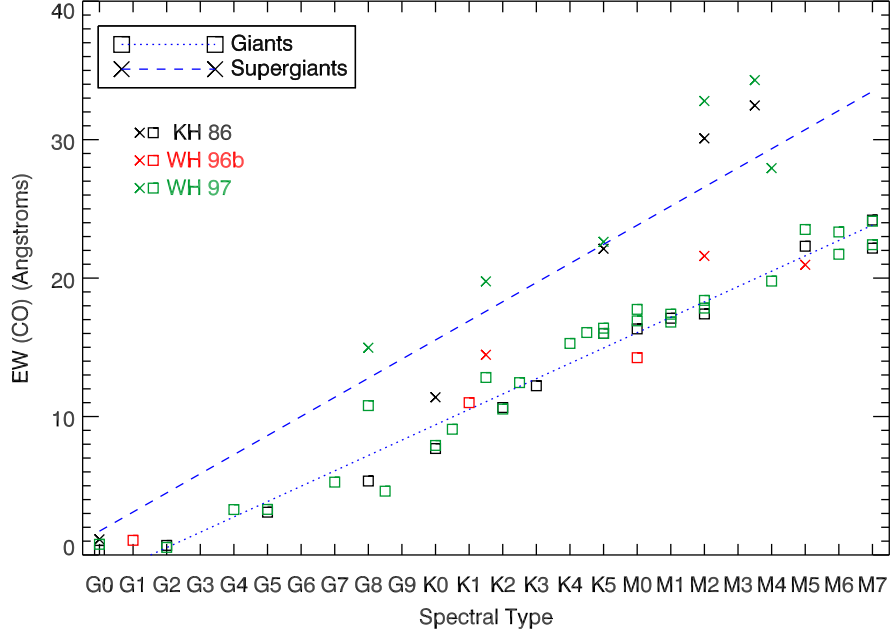
Fig. 2.—: Relationship between spectral-type and the equivalent width of the CO bandhead feature, deduced from template spectra of Kleinmann & Hall (1986), Wallace & Hinkle (1996b) and Wallace & Hinkle (1997). Giants are plotted as squares, supergiants as crosses. The dotted and dashed lines show linear fits through the data. These fits were used to determine the spectral types of the target stars.

### 2.4.2. Radial velocity measurements

Following the method described in detail by Figer et al. (2003), accurate radial velocities were measured by cross-correlating the complex stellar CO bandhead feature beginning at $\sim 2.293\mu$m with that of Arcturus, from the spectrum of Wallace & Hinkle (1996a) shifted to the zero local standard of rest velocity. We experimented with using different wavelength regions for the cross-correlation, such as including/excluding the sharp edge at the blue-edge, to test the robustness of the measurement. We found that our velocity measurements are stable to within $\pm 1\,$km s$^{-1}$ regardless of the wavelength range used, therefore the absolute uncertainty of any velocity measurement is dominated by the $\pm 4\,$km s$^{-1}$ error in the wavelength solution.

Figer et al. (2003) concluded that this method, when applied to Red Giants, introduced a systematic error in the measured radial velocity as a function of $EW_{\rm CO}$, and accounted for $\pm 2\,$km s$^{-1}$ across the full range of observed $EW_{\rm CO}$. In order to assess any impact this may have on our data, we applied the method to the high-resolution template spectra of RSGs presented in Wallace & Hinkle (1997). As these spectra are few, it was inconclusive
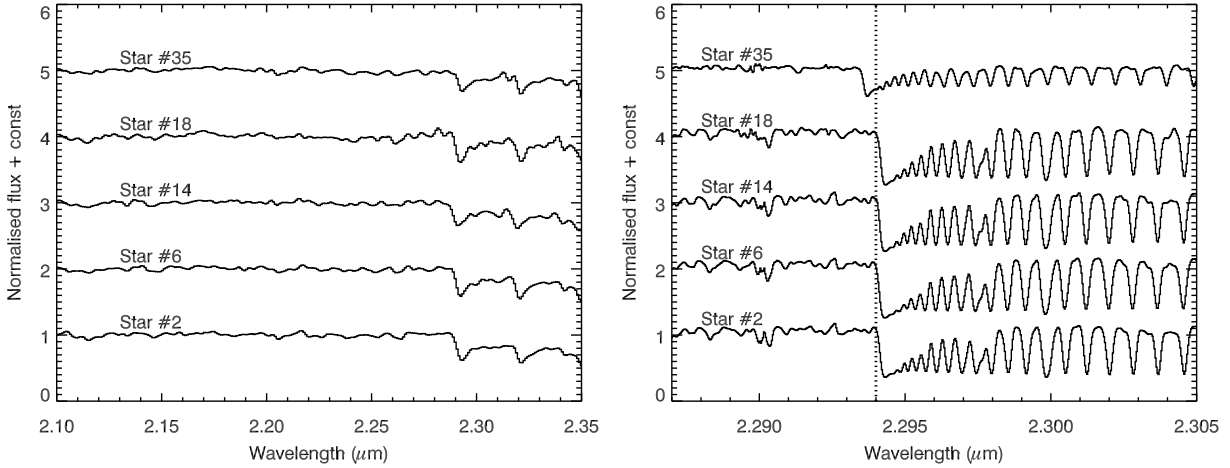
**Fig. 3.**—: Examples of the spectra. *Left:* the *IRMOS* data, clearly showing the CO bandhead absorption – indicative of late spectral-types. *Right:* the *NIRSPEC* follow-up data, which highlights the radial velocity differences between Star 35 and the rest.

as to whether this systematic trend of measured $v_{\rm rad}$ with $EW_{\rm CO}$ is present in our data, but if so it would appear to be very small ($\pm 1\,{\rm km\ s^{-1}}$). It does not therefore contribute significantly to the absolute uncertainty of individual radial velocity measurements. It may however have an impact on the internal error between measurements, and become important when determining the cluster's virial mass. We will make a more comprehensive discussion of the effect of including this uncertainty in Sect. 4.1.1.

## 3. Results

### 3.1. Spectra

Examples of the NIR spectra are shown in Fig. 3. From the *IRMOS* data (Fig. 3, *left*), the CO bandhead absorption can clearly be seen in the spectra, implying late spectra types for the stars. Also, no stars show the 'vignetting' at the edges of the $K$-band, indicative of the $H_2O$ absorption often seen in Red Giants (see e.g. atlas of Kleinmann & Hall 1986), though we note that care should be taken using this selection criterion in uncalibrated spectra. We therefore identify these stars as *candidate* RSGs. We found stars displaying these features down to $K_S \lesssim 7.5$.

The follow-up *NIRSPEC* data of these stars are shown in Fig. 3 (*right*), and show the blue-edge of the feature in greater detail. Here, the difference between Star 35 and the others
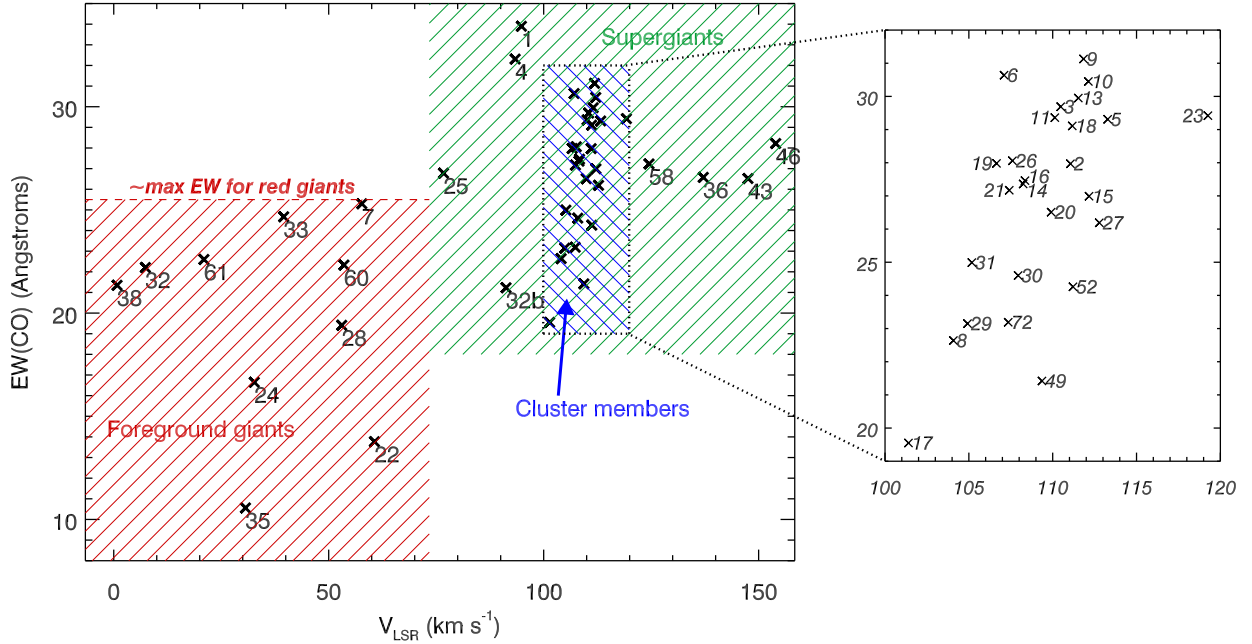
**Fig. 4.**—: Plot of CO equivalent width versus $v_{\mathrm{LSR}}$ for all stars observed with *NIRSPEC*. Stars in the cross-hatched region have very similar velocities, and are likely to be part of the same cluster. Stars in the bottom-left are probably foreground stars due to their low $W_\lambda$ and much lower velocities.

shown in the plot is obvious – it can be seen from the blue-edge of the CO bandhead feature (indicated by the dotted line) Stars 2, 6, 14 and 18 have very similar velocities. Star 35 however, has a notable velocity-shift with respect to the others. In the following section, we use the radial velocity and CO equivalent width measurements to argue that, of the stars observed, a total of 26 can be readily identified as being part of a physical association of RSGs.

## 3.2. Supergiants vs. foreground stars

The observed stars in this field separate into three categories: physically-associated cluster members, unrelated foreground/background RSGs, and foreground M giants and dwarfs. Here we use the observational data from the high-resolution spectroscopy to determine which stars lie in which of these categories.

Figure 4 shows a plot of CO bandhead equivalent width ($W_\lambda$) against radial velocity. Marked on the plot is the maximum $EW_{\mathrm{CO}}$ of the CO bandhead feature observed in M

**Table 2::** Derived data of the cluster stars. (1): Star ID, in order of ascending brightness in $K_S$; (2): radial velocity – absolute uncertainty is $\pm4\,\mathrm{km\,s^{-1}}$, internal error is $\pm1\,\mathrm{km\,s^{-1}}$; (3 & 4): effective temperature and spectral type, accurate to 2 subtypes (temperatures taken from Levesque et al. 2005); (5): $K$-band extinction; (6) absolute magnitude; (7): Luminosity.

| (1) | (2) | (3) | (4) | (5) | (6) | (7) |
|-----|-----|-----|-----|-----|-----|-----|
| ID | $V_{\mathrm{LSR}}$ ($\mathrm{km\,s^{-1}}$) | $T_{\mathrm{eff}}$ (K) | Spec Type | $A_{K_S}$ | $M_K$ | $\log(L_{bol}/L_\odot)$ |
| 2 | 111.1 | 3605±147 | M3 | 1.39±0.06 | $-11.12^{+0.33}_{-0.63}$ | $5.22^{+0.25}_{-0.13}$ |
| 3 | 110.5 | 3535±130 | M4 | 1.34±0.07 | $-10.72^{+0.33}_{-0.63}$ | $5.04^{+0.25}_{-0.13}$ |
| 5 | 113.3 | 3535±130 | M4 | 1.99±0.07 | $-11.02^{+0.33}_{-0.63}$ | $5.16^{+0.25}_{-0.13}$ |
| 6 | 107.1 | 3450±100 | M5 | 1.17±0.08 | $-9.95^{+0.32}_{-0.63}$ | $4.70^{+0.25}_{-0.13}$ |
| 8 | 104.1 | 3840±135 | K5 | 1.45±0.09 | $-10.23^{+0.32}_{-0.63}$ | $4.94^{+0.25}_{-0.13}$ |
| 9 | 111.8 | 3450±100 | M5 | 1.64±0.08 | $-10.28^{+0.32}_{-0.63}$ | $4.84^{+0.25}_{-0.13}$ |
| 10 | 112.1 | 3450±100 | M5 | 1.42±0.08 | $-10.03^{+0.32}_{-0.63}$ | $4.73^{+0.25}_{-0.13}$ |
| 11 | 110.1 | 3535±130 | M4 | 1.42±0.08 | $-10.08^{+0.33}_{-0.63}$ | $4.78^{+0.25}_{-0.13}$ |
| 13 | 111.5 | 3535±130 | M4 | 1.42±0.07 | $-9.85^{+0.33}_{-0.63}$ | $4.69^{+0.25}_{-0.13}$ |
| 14 | 108.2 | 3605±147 | M3 | 1.39±0.06 | $-9.77^{+0.33}_{-0.63}$ | $4.68^{+0.25}_{-0.13}$ |
| 15 | 112.2 | 3660±127 | M2 | 1.27±0.06 | $-9.59^{+0.32}_{-0.63}$ | $4.63^{+0.25}_{-0.13}$ |
| 16 | 108.3 | 3605±147 | M3 | 1.25±0.06 | $-9.50^{+0.33}_{-0.63}$ | $4.57^{+0.25}_{-0.13}$ |
| 17 | 101.4 | 4015±130 | K3 | 1.77±0.05 | $-9.99^{+0.31}_{-0.62}$ | $4.90^{+0.25}_{-0.12}$ |
| 18 | 111.2 | 3535±130 | M4 | 1.16±0.07 | $-9.36^{+0.33}_{-0.63}$ | $4.50^{+0.25}_{-0.13}$ |
| 19 | 106.7 | 3605±147 | M3 | 1.12±0.06 | $-9.17^{+0.33}_{-0.63}$ | $4.44^{+0.25}_{-0.13}$ |
| 20 | 109.9 | 3660±127 | M2 | 1.30±0.06 | $-9.32^{+0.32}_{-0.63}$ | $4.52^{+0.25}_{-0.13}$ |
| 21 | 107.4 | 3660±127 | M2 | 1.79±0.06 | $-9.81^{+0.32}_{-0.63}$ | $4.71^{+0.25}_{-0.13}$ |
| 23 | 119.3 | 3535±130 | M4 | 2.29±0.07 | $-10.35^{+0.33}_{-0.63}$ | $4.89^{+0.25}_{-0.13}$ |
| 26 | 107.6 | 3605±147 | M3 | 1.31±0.06 | $-9.16^{+0.33}_{-0.63}$ | $4.44^{+0.25}_{-0.13}$ |
| 27 | 112.8 | 3660±127 | M2 | 1.45±0.06 | $-9.19^{+0.32}_{-0.63}$ | $4.47^{+0.25}_{-0.13}$ |
| 29 | 104.9 | 3790±130 | M0 | 1.14±0.08 | $-8.86^{+0.33}_{-0.63}$ | $4.38^{+0.25}_{-0.13}$ |
| 30 | 107.9 | 3745±117 | M1 | 1.15±0.09 | $-8.82^{+0.32}_{-0.63}$ | $4.35^{+0.25}_{-0.13}$ |
| 31 | 105.2 | 3745±117 | M1 | 1.62±0.09 | $-9.24^{+0.32}_{-0.63}$ | $4.51^{+0.25}_{-0.13}$ |
| 49 | 109.4 | 3920±112 | K4 | 4.58±0.22 | $-11.30^{+0.38}_{-0.66}$ | $5.39^{+0.26}_{-0.15}$ |
| 52 | 111.2 | 3790±130 | M0 | 2.24±0.08 | $-8.72^{+0.33}_{-0.63}$ | $4.32^{+0.25}_{-0.13}$ |
| 72 | 107.3 | 3790±130 | M0 | 2.55±0.16 | $-8.62^{+0.36}_{-0.64}$ | $4.28^{+0.26}_{-0.14}$ |
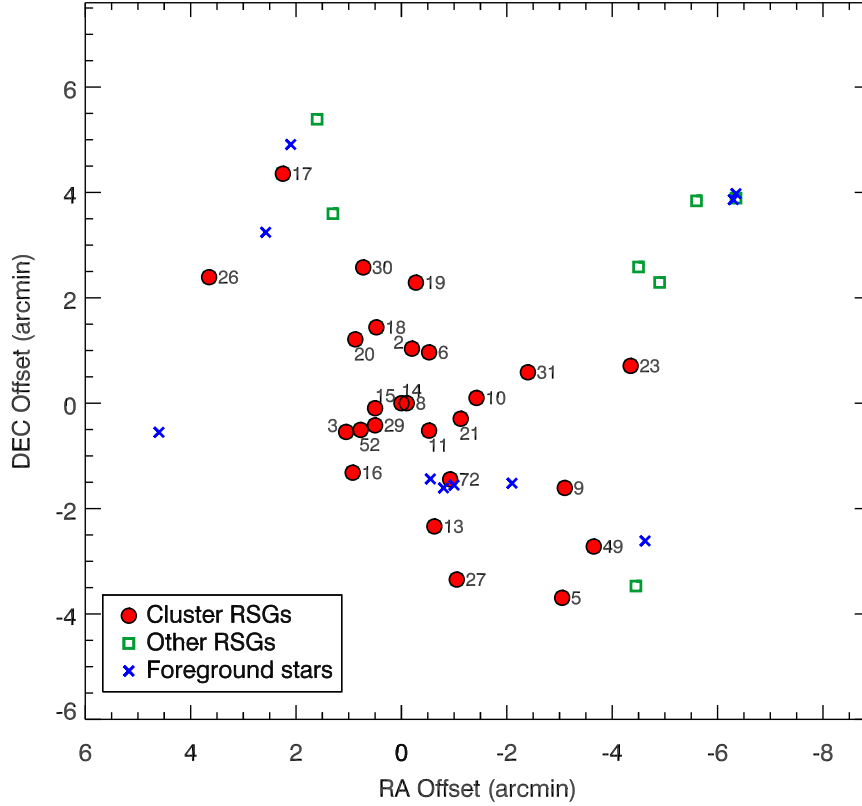
**Fig. 5.—:** Illustration of the location of the stars belonging to the cluster, and foreground/background objects.

giants. Any stars above this line are therefore likely to be supergiants. The plot shows that there are no stars with high-$EW_{CO}$ at low radial velocities, just as there are no stars with low-$EW_{CO}$ at high-$v_{rad}$. We thus identify those stars in the lower-left of the plot (red crosshatched region) as foreground stars; while those stars in the upper-right, with higher $v_{rad}$ and $EW_{CO}$, are identified as more-distant supergiants.

Notice that within this subsample of 'supergiants', there is a tight grouping of many stars with radial velocities 100–120 km s$^{-1}$. We identify the 26 stars within this grouping (crosshatched region) as being part of a physical association. A cluster member with a velocity outside this range would imply a large runaway speed, and would be unlikely to remain in the field-of-view for a likely cluster age of ∼10Myr (see Sect.4.2). The supergiants ouside this region are therefore probably unrelated objects in the same line-of-sight along the base of the Scutum-Crux arm. It will be shown later that these objects are typically more reddened, supporting this conclusion (see Sect. 3.5). There is of course the possibility that the sample of 26 'cluster' stars is contaminated by other RSGs along the line-of-sight with

peculiar velocities, making them appear to be part of the cluster. This number is difficult to quantify, but from the velocity-spread of the 'unrelated' supergiants it would seem unlikely that there more than one or two interlopers.

From these selection criteria, we determine that the cluster contains 26 RSGs – the largest associated population of RSGs discovered to date and almost twice as many as in the nearby RSGC1 described in FMR06. We also identify a further 8 RSG candidates along the line-of-sight to RSGC2, based on the stars' high CO equivalent widths. The location of these stars within the field of the cluster is illustrated in Fig. 5.

Aside from Stars 12 & 34, our high-resolution observations are complete down to $K_S$ <6.6. Of the 33 stars brighter than this threshold, 23 are determined to be cluster members. Of the stars we sampled fainter than this threshold, only 3 of 11 stars were found to belong to the cluster. Hence the cluster RSGs tend to be among the brighter stars in the field, and it is unlikely that a significant number of cluster RSGs (more than one or two) were missed in our survey of the cluster.

### 3.3. Spectral types

We take the stars classified as supergiants and determine their spectral types based on the relation to CO-bandhead equivalent width derived in Sect. 2.4. The spectral types are listed in Table 2, and are plotted in a histogram in Fig. 6. We plot both the entire sample of supergiants, and the subsample of cluster members (cross-hatched). The median spectral-type for both samples is M3 I, which is in agreement with the average spectral type in the Galaxy (M2) and that of the nearby RSGC1 cluster (M3) (Elias et al. 1985, FMR06).

The median spectral-type of RSGs is thought to be linked to chemical abundance. For example, RSG distribution in the low-metallicity environments of the Magallic Clouds is significantly different to that of the Galaxy. Median spectral-types of K5, M1, and M2 have been found from studies of the SMC, LMC and the Galaxy respectively (Humphreys 1979; Elias et al. 1985; Massey & Olsen 2003). This difference is thought to arise either from the metallicity-dependent opacity of the stellar envelope (Elias et al. 1985), or the abundance-sensitive strengths of diagnostic molecular absorption features, e.g. TiO bands (Massey & Olsen 2003). Either way, that the median spectral-types of the clusters RSGC1 and 2 agree with i) each other, and ii) those in the rest of the Galaxy, suggests that these objects have roughly similar metallicities to the Galactic average.
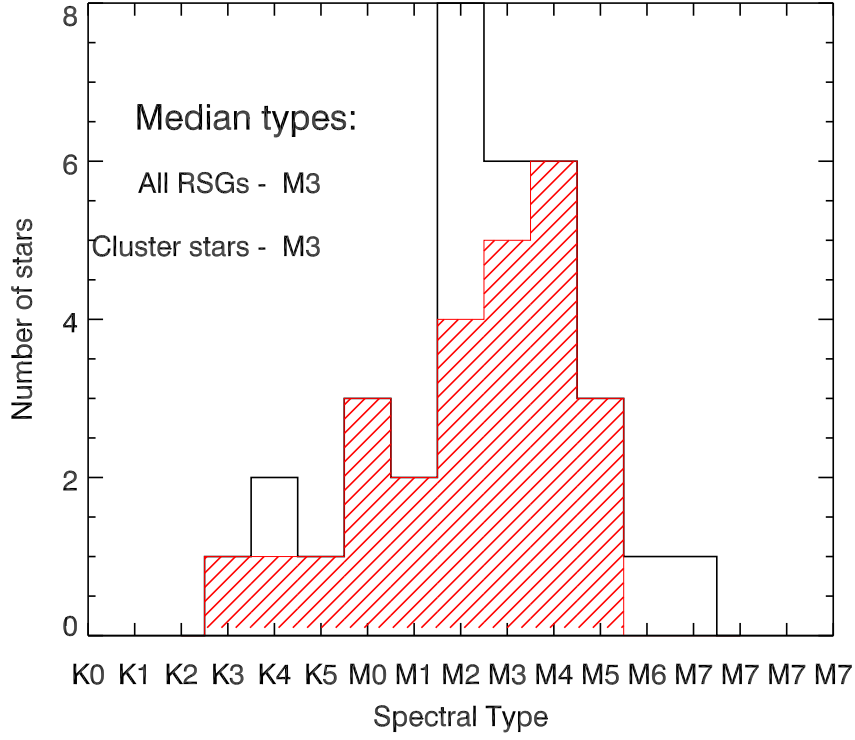
**Fig. 6.**—: Histogram of the spectral types of the stars identified as supergiants, and the subsample determined to be 'cluster members' (cross-hatched region). The median type of both subsamples (M3) is consistent with the nearby RSG cluster RSGC1 (M3, FMR06) and the rest of the Galaxy (M2, Elias et al. 1985).

## 3.4. Cluster distance

The mean radial velocity of the cluster subsample is $\bar{v}_{LSR} = 109.3 \pm 0.7 \, \mathrm{km \, s^{-1}}$, with the uncertainty taken from Poisson statistics of the 26 stars. The cluster radial velocity is constrained extremely well by the large number of measurements, and the uncertainty in this value is dominated by the precision of the wavelength solution, $\pm 4 \, \mathrm{km \, s^{-1}}$.

In converting this radial velocity into a kinematic distance to the cluster, we are limited by the uncertainties in the Galactic rotation curve. We use the most contemporary measurements of the Galactic centre distance and solar rotational velocity as compiled by Kothes & Dougherty (2007, in press). In determining the distance to Wd 1, these authors used the Galactic centre distance $D_{\mathrm{GAL}} = 7.6 \pm 0.3$ kpc, as determined by Eisenhauer et al. (2005), and the solar rotation velocity of $\Theta_{\odot} = 214 \pm 7 \, \mathrm{km \, s^{-1}}$, averaged from measurements by Reid & Brunthaler (2004) and Feast & Whitelock (1997). We use these values to construct the Galactic rotation curve in the direction of RSGC2 shown in Fig. 7.
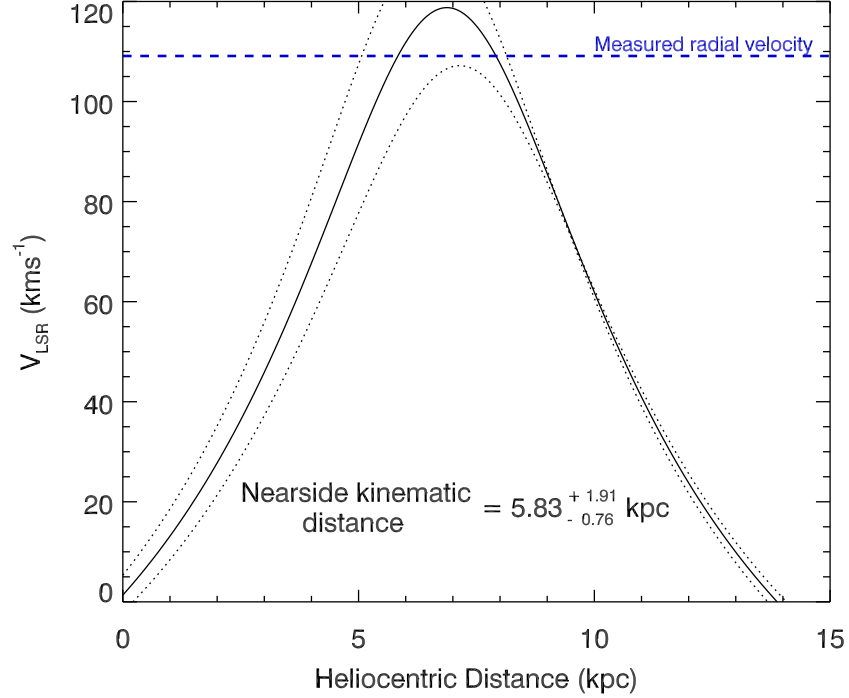
**Fig. 7.**—: Galactic rotation curve in the direction of RSGC2, using the latest measurements collated by Kothes & Dougherty (2007) (solid-line). The dashed-line represents the mean radial velocity of the cluster stars, implying the kinematic distance marked on the plot. Dotted-lines illustrate the errors in this distance implied by uncertainties in the solar rotational velocity and the distance to the Galactic centre.

From comparison with the cluster's radial velocity, we derive a kinematic distance of $5.83^{+1.91}_{-0.78}$ kpc. The uncertainties are determined from the minimal and maximal nearside distance from the errors in $D_{\mathrm{GAL}}$ and $\Theta_\odot$, and are rather large due to the location of the cluster close to the tangential point of the Galactic arm (see Fig. 7).

This distance estimate is considerably closer than the ~30kpc quoted in S90. This greater distance was determined by assuming that the cluster stars were M supergiants, then calculating the distance modulus based on their typical absolute magnitudes. However, S90 did not take into account interstellar extinction, which we determine to be $A_V = 13.1$ assuming the interstellar extinction law of Rieke & Lebofsky (1985) (see Sect. 3.5). This explains S90's large distance overestimate.

In a separate study, Nakaya et al. (2001) derived a much closer distance estimate – they isolated a sample of stars which appeared to be reddened in their $I$ vs. $R - I$ colour-magnitude diagram, and assumed these were early-type stars belonging to the cluster. They

then dereddened these stars to the intrinsic colours of A0 stars, deriving an extinction of $A_V = 11.4$. Upon fitting the 'A0' stars and the S90 'red' stars with a model isochrone, they finally arrived at a distance of 1.5kpc. In analysis of similar data, Ortolani et al. (2002) derived a distance of 6kpc, by adding the constraint that the cluster containing so many RSGs cannot be older than $\sim$20Myr.

While Ortolani et al.'s distance estimate is comparable to ours, these studies highlight the problematic nature of inferring cluster properties from photometry alone. Our method of determining the distance to the cluster is much more direct and relies less on assumptions of cluster membership and spectral types. From the radial velocity data, the grouping of so many stars with a velocity rms of $\pm 3.5\,\mathrm{km\ s^{-1}}$ is strong evidence that these stars are associated. Even allowing for a peculiar cluster velocity of $\pm 20\,\mathrm{km\ s^{-1}}$ from the Galactic rotation curve, due to e.g. the cluster's proximity to the Galactic bulge, this would still only imply an extra uncertainty of $\pm$1kpc.

## 3.5. Extinction

Figure 8 shows a 2MASS colour-magnitude diagram of all stars with $7'$ of the cluster centre, which is taken to be the position of Star 14 (see Table 1). The stars classified as cluster members are plotted as circles, the unrelated supergiants as triangles, and the foreground stars as squares. An $A_K = 1$ reddening vector is plotted, and to guide the eye a 12Myr solar metallicity isochrone is shown (Schaerer et al. 1993), which has been dereddened by $A_K = 1.47$ (see below).

It can be seen that the majority of the cluster stars are grouped tightly at the top of the isochrone, with no cluster stars located significantly to the left of the isochrone – consistent with the sample being uncontaminated by foreground stars. The cluster stars significantly to the right of the isochrone all lie along a reddening vector from this core grouping, suggesting that extra circumstellar reddening exists for these objects. A 2MASS colour-colour diagram is shown in Fig. 9. Again, the majority of the cluster stars form a tight grouping, and are located along the reddening vector from the origin.

To determine the extinction to the cluster, we de-redden each cluster star to the intrinsic colours appropriate for their spectral type and a luminosity class of Iab, according to the survey of Galactic RSGs by Elias et al. (1985). From the $(J - K_S)$ and $(H - K_S)$ colour excesses of each star, we determine the extinction $A_{K_S}$ towards each star using the relation in Rieke & Lebofsky (1985):
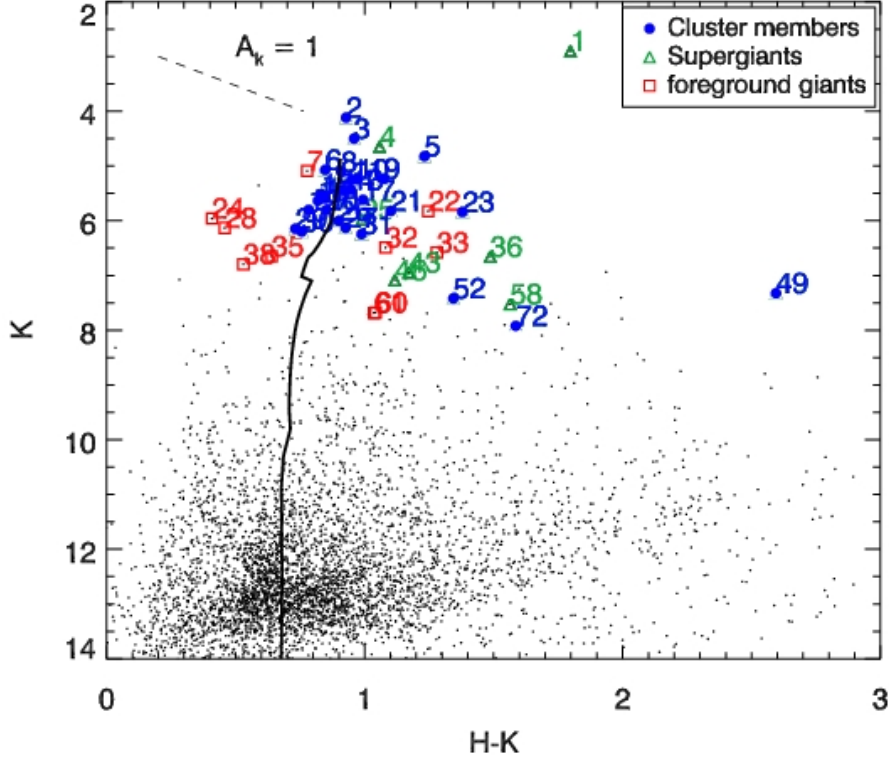
**Fig. 8.—:** Colour – magnitude diagram for all stars in the *2MASS* point-source catalogue within 7′ of the cluster center (*dots*). The stars observed in this paper are plotted with their ID# as indicated in the legend. The solid line represents a 12Myr isochrone from Geneva models with solar metallicity and canonical mass-loss rates, which has been reddened according to the interstellar extinction-law of Rieke & Lebofsky (1985) with $A_K = 1.47$. A reddening vector of $A_K = 1$ is also plotted. The majority of the cluster stars form a tight grouping at the top of the isochrone, the location of RSGs.

$$A_{K_S} = \frac{E_{\lambda - K_S}}{(\lambda/\lambda_{K_S})^{-1.53} - 1} \tag{1}$$

The uncertainty in each star's extinction is governed by the error in its spectral-type. For $\pm 2$ subtypes, then from the variations in RSG intrinsic colours the uncertainty in the $A_K$ measurement of each star is about $\pm 0.06$. This is consistent with the differences we find in the extinction measurements using the two different colour-excesses (see below).

From the measurements of all the stars, we find the median extinction towards the cluster to be $A_{K_S}(J - K_S) = 1.462$, and $A_{K_S}(H - K_S) = 1.424$. These two measurements are consistent with one another, and we adopt the average of these measurements, $A_{K_S} = 1.44 \pm 0.02$, and hence $A_V = 12.9 \pm 0.2$, to be the extinction towards RSGC2. The measured
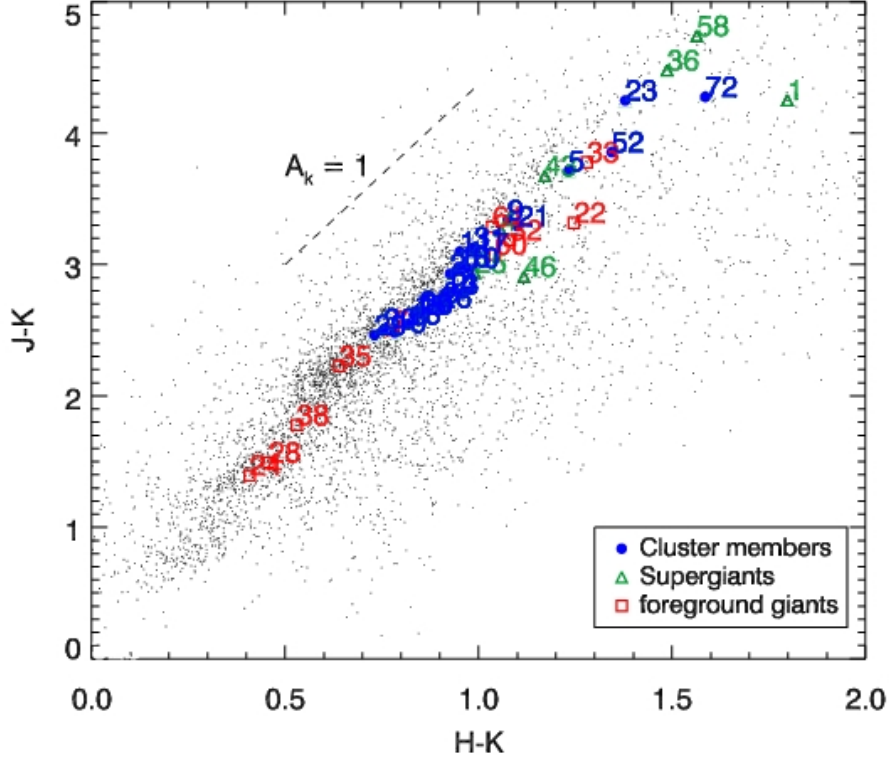
**Fig. 9.**—: *2MASS* colour-colour diagram of the stars plotted in Fig. 8, with the same plotting symbols. A reddening vector according to $A_K = 1$ is plotted. For clarity, Star 49 – which lies along the reddening vector from the cluster stars with an extinction $A_K = 4.58$ – is not shown.

extinction towards the individual stars, and the associated uncertainty determined from the error in spectral-type, is listed in Table 2.

As mentioned in Sect. 3.4, this extinction is slightly higher than that derived by Nakaya et al. (2001), who found $A_V = 11.2$. Their extinction estimate was based on the assumption that a collection of stars with particular $R - I$ colours were cluster members and had mean spectral-type A0. As we know the spectral types of the stars to within a subtype, and are able to take the median of many stars which we are confident are cluster members, we consider ours to be a much more reliable estimate.

From Table 2, we see that the extinction towards the individual stars varies substantially across the field. In particular, Star 49 is significantly more obscurred than the rest, with $A_{K_S} = 4.6$. In the case of this star, the extra extinction can be readily associated with mid-IR excess, and is likely due to circumstellar material (see Sects. 3.6 and 4.3). For the other stars with extra extinction, such as Stars 5, 23, 52 and 72, an association with mid-IR excess is less obvious: #5 and #23 have only modest excess (see Fig. 22), while #52 and

#72 are not detected in *MSX*. These anomalies may arise due to a combination of factors: there may be significant non-uniformity in the foreground extinction, indeed it can be seen in Fig. 19 that there is much diffuse $8\mu$m emission over the field (with #23 appearing to be spatially-coincident with a dark-lane); source-confusion in the *MSX* images may make it impossible to detect fainter stars in crowded regions, in particular #52, which is dwarfed by emission from the nearby #6, may suffer from this effect; and finally we cannot entirely discount that the sample of 'cluster' stars is contaminated by one or two background stars with peculiar velocities, which are extincted by an increased column-density of interstellar material (see also Sect. 3.2).

### 3.6.   Luminosities and spectral energy distributions

From each stars' extinction and the kinematic distance of the cluster, we calculate absolute magnitude of each star $M_{K_S}$. We then interpolate the bolometric correction $BC_K$ for each star's temperature, according to the recently re-derived values of Levesque et al. (2005), to estimate their bolometric luminosities. These results are listed in Table 2.

The uncertainties in $L_{\rm Bol}$ are derived from the quadrature sum of the errors in $A_K$, $BC_K$, and the cluster distance, $D_{\rm cl}$. The errors in $A_K$ and $BC_K$ are governed by the precision to which we can determine the stars' spectral types, i.e. $\pm 2$ subtypes. While these uncertainties are small compared to that in $D_{\rm cl}$, we can be confident that the stars are all at the *same* distance. Hence, the propagation of the error in spectral-type through to that in $L_{\rm Bol}$ will be important when investigating the luminosity spread of the RSGs and the age of the cluster.

In addition to the *2MASS* photometry, we also identify these stars in the point-source catalogues of *Spitzer/GLIMPSE* (Benjamin et al. 2003) and *MSX* (Egan et al. 2001). In the *GLIMPSE* catalogue, many of the stars are too bright to be included in the high-precision version of the catalogue, and instead only appear in the less-accurate, 'more-complete' version. In the case of the *MSX* data, despite the large beamsize ($\sim 18''$), the cluster is open enough to get unambiguous photometry on several of the stars.

In Fig. 22 (Appendix A) we plot the spectral energy distributions (SEDs) of the cluster stars. We de-redden the fluxes of the stars according to the extinction $A_{K_S}$ towards each star, in combination with the interstellar extinction law for *GLIMPSE* and *MSX* photometry as defined in Indebetouw et al. (2005) and Messineo et al. (2005) respectively. The raw photometry is plotted as crosses, and the dereddened as filled circles.

Plotted over the photometry are black-body curves appropriate for stars' temperatures, absolute $K$-band magnitudes and the nearside kinematic distance to the cluster. For the

majority of the stars, the black-body curves provide good fits to the dereddened photometry up to $8\mu$m, and validates our empirical method of determining the star's temperatures. Some objects, e.g. Stars 19, 20 and 21, appear to be under-luminous at $4.3\mu$m. This can be understood as being due to dense molecular absorption bands in this wavelength range, which can readily be seen in spectral-type M model-atmospheres (e.g. Fluks et al. 1994).

In the mid-IR photometry of *MSX*, many stars show evidence of significant excess emission, particularly at $12\mu$m. This mid-IR excess is common to RSGs, and is due to the large amounts of circumstellar oxygen-rich dust produced in this high mass-losing phase. The excess emission is illustrated in the dereddened *2MASS-MSX* colour-magnitude diagrams shown in Fig. 10. As these unreddened photospheric colours should be approximately zero, positive *2MASS-MSX* indices are indicative of dusty circumstellar ejecta.

Whitelock et al. (1994) showed that the $K - [12]$ colour from *IRAS* photometry was directly proportional to mass-loss rate for AGB stars. This colour may be the most effective diagnostic for RSG mass-loss rates, as it will be influenced by the broad silicate emission feature at $\sim$9–12$\mu$m often seen in RSG spectra (Buchanan et al. 2006). As RSGs' mass-loss rates are roughly proportional to their luminosity (van Loon et al. 2005), in Fig. 10 we plot the bolometric magnitude of the stars against their *K-MSX* colours. Each plot shows the expected $\sim$linear trend of redder colours for increasingly brighter stars, which was also seen in a sample of Galactic RSGs by Massey et al. (2005) when using the data from Josselin et al. (2000) and re-deriving the stellar distances.

Another effective measure of mass-loss rate may be the [8]-[12] (*MSX A-C*) colour. This measures not just the mid-IR excess, but specifically the amount of excess caused by the broad silicate dust feature. Figure 11 plots absolute bolometric magnitude against this colour, and shows a clear relation of increasing $12\mu$m excess with increasing luminosity. A comprehensive study of the empirically-derived mass-loss rates of both the RSG clusters is beyond the scope of this work, and will be the subject of a future paper.

## 4. Discussion

### 4.1. Initial mass

To determine the initial mass of the cluster, we use two independent methods. In Sect. 4.1.1 we use our high-precision radial velocity measurements to infer the cluster's virial mass, under the assumption that it is in dynamical equilibrium. Secondly, in Sect. 4.1.2 we compare this measurement with that determined from simulations of clusters with large numbers of RSGs, using stellar evolution models.
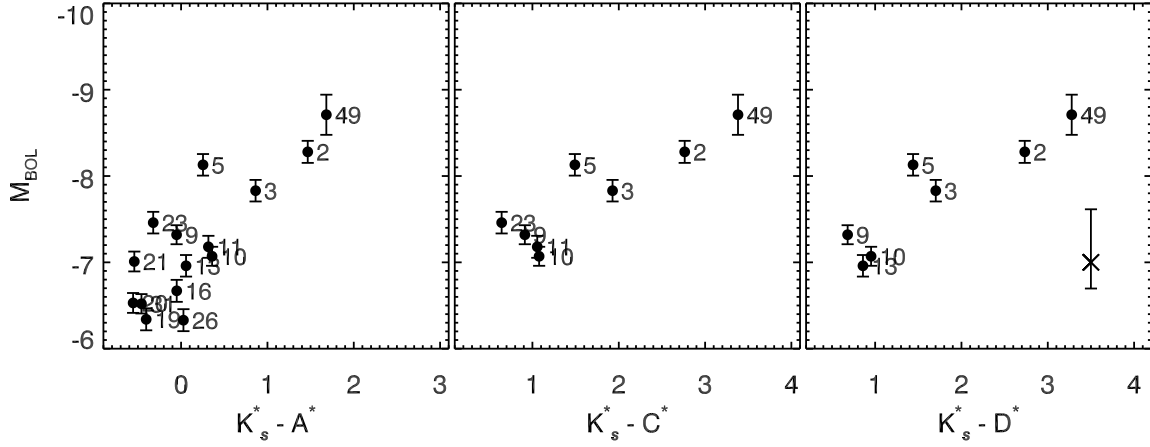
**Fig. 10.**—: *2MASS-MSX* colour-magnitude diagrams. The plots show the cluster stars' bolometric absolute magnitude against *dereddened* $K_S$-$(A, C, D)$ colours. Errors in $M_{\mathrm{Bol}}$ are shown which discount the error in cluster distance – when included the average error size is indicated by the error bar in the bottom-right of the far-right panel. Errors in colour are of order the size of the plotting symbols.
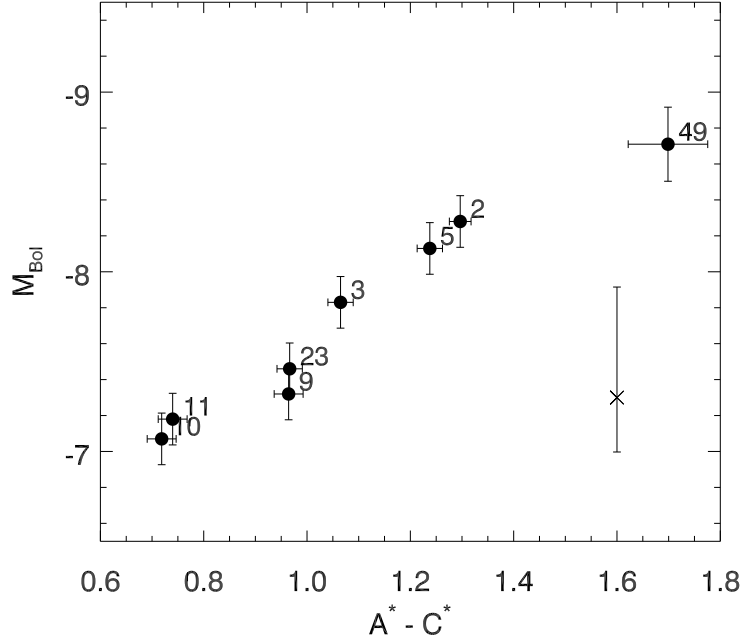


**Fig. 11.**—: Absolute magnitude versus unreddened $A - C$ colour, illustrating the trend of increasing [8]-[12] excess with luminosity for the cluster RSGs. The errors in $M_{\mathrm{Bol}}$ do not include the uncertainty in the cluster distance, which is illustrated by the error-bar in the lower right.

### 4.1.1. Virial mass

Following the method of Mengel et al. (2002), the mass of the cluster can be measured under the assumption that it is in dynamical equilibrium. Below, we use the dispersion in radial velocity from the high-resolution spectra to estimate the dynamical mass of RSGC2. As a caveat, we note that recent work by Bastian & Goodwin (2006) suggests that young massive clusters ($\lesssim 50\mathrm{Myr}$, $\gtrsim 10^4 M_\odot$) can be *out* of virial equilibrium. This is caused by the violent relaxation of the cluster following the ejection of the left-over interstellar natal material by the first supernovae. As a result, the cluster mass can be overestimated by factors of up to $\sim$3 if it is incorrectly assumed to be virialized. With this in mind, we consider our derived virial mass to be an order-of-magnitude estimate.

From the radial velocity dispersion $\sigma_v$, we can estimate the dynamical cluster-mass $M_{\mathrm{dyn}}$ from the relation,

$$M_{\mathrm{dyn}} = \frac{\eta \sigma_v^2 r_{\mathrm{hp}}}{G} \qquad (2)$$

where $r_{\mathrm{hp}}$ is the half-light radius of the cluster, $G$ is the gravitational constant, and $\eta$ is a constant which depends on the density and $M/L$ as a function of radius, and is typically in the range 5-10 (for a review of the parameter $\eta$ see Introduction of Mengel et al. 2002). Below, we discuss our measurements of the parameters in this relation and estimate the dynamical mass of RSGC2.

**Velocity dispersion:** As mentioned in Sect. 2.4, the method we use to determine accurate radial velocities from the CO bandhead feature was noted by Figer et al. (2003) to introduce a systematic offset as a function of $W_\lambda$ when applied to Red Giants. This offset was determined from measurements of template Red Giants with well-known radial velocities. From the few template spectra of RSGs, it appears that the effect of this systematic uncertainty is less than $\pm 2\,\mathrm{km\ s^{-1}}$ in our data, over the full range of equivalent widths.

To investigate this further, in Fig. 12 we plot the radial velocity of the 'cluster-members' against their equivalent widths. The radial velocities have been shifted by the mean velocity of all the stars, to illustrate the width of the dispersion. There is an apparent trend of velocity with $EW_{\mathrm{CO}}$, which has a Pearson correlation coefficient of 0.5 when a linear relationship is assumed, and is plotted over the data. There is no reason to expect a real trend to exist between velocity and equivalent width, therefore we suspect that this relation may be an artifact of our velocity-measuring method.

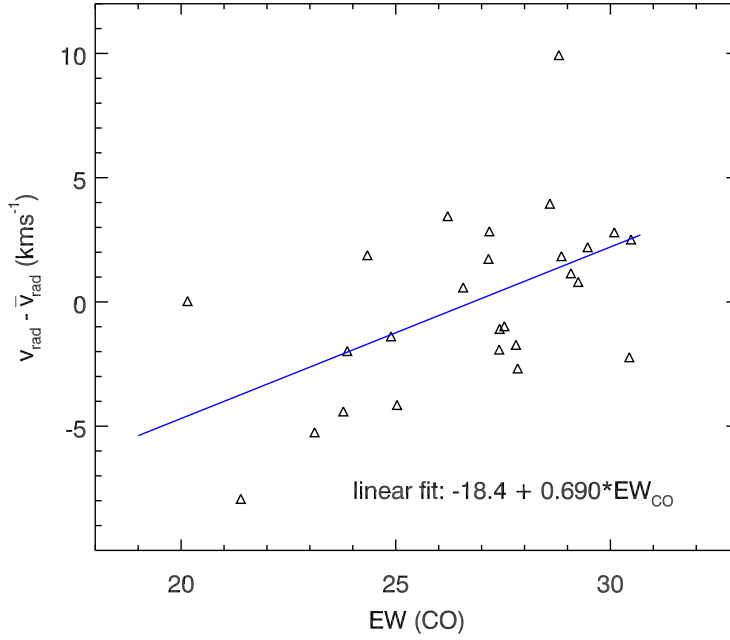We investigate the effects of taking two differing estimates for the velocity dispersion:

**Fig. 12.**—: Cluster velocity dispersion as a function of equivalent width of the CO bandhead feature. The slight trend may be an artifact of the method used to determine the radial velocities of the stars.

the *maximal* (observed) dispersion, and the *minimal* dispersion when the linear relation shown in Fig. 12 is corrected for. In each of these estimates we have subtracted the internal uncertainty in each measurement ($\pm 1 \, \text{km s}^{-1}$) in quadrature. We measure the uncorrected data, i.e. that plotted in Fig. 12, to have a $1\sigma$ dispersion of $3.4 \, \text{km s}^{-1}$; while the 'corrected' velocities have $1\sigma$ dispersion of $2.8 \, \text{km s}^{-1}$. Therefore, we estimate that if any systematic uncertainty exists, its effect is at most $\pm 20\%$. We illustrate the 'corrected' velocity dispersion of the cluster in Fig. 13. The plot seems to be a trend of postitive velocities in the south-west and positive in the north-east, consistent with a rotating self-gravitating cluster

**Half-light radius:** As this cluster is much more 'open' than its neighbour RSGC1, the half-light radius is more difficult to define. To measure this quatity, we make the assumption that the RSGs are representative of the density profile of the cluster. Should mass-segregation exist in the cluster, this will be an underestimate. Figure 14 plots the cumulative luminosity distribution of the stars in the cluster, assuming that the mean of the star positions ($18^h$ $39'$ $17.9''$, $-6°2'$ $3.3''$) is the cluster centre. The plot indicates the cluster half-light radius is around $(1.9\pm0.3)'$. It was found that adjusting the position of the cluster centre by $\pm0.5'$ did not significantly affect this value with respect to the quoted uncertainty.
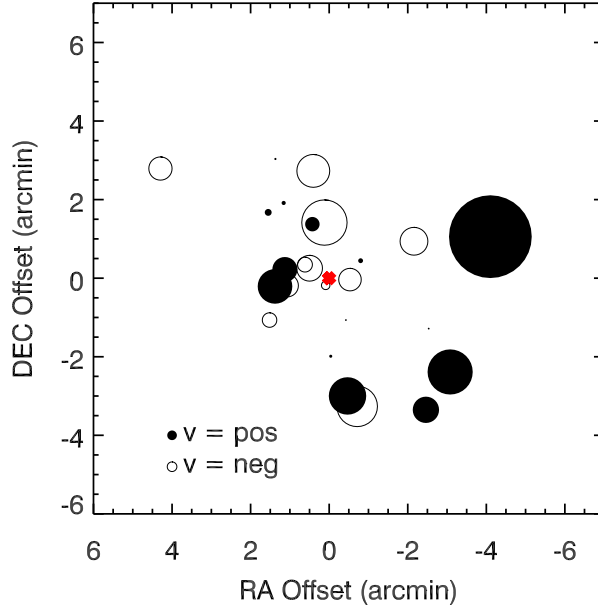
Fig. 13.—: Illustration of the velocity dispersion of the stars in the cluster, when the trend with equivalent width has been corrected for and the mean cluster velocity subtracted. Symbol sizes are proportional to absolute velocity of each star, open symbols representing negative velocities and filled symbols positive velocities. The cross denotes the cluster 'centre', defined as the mean of the positions of the stars.
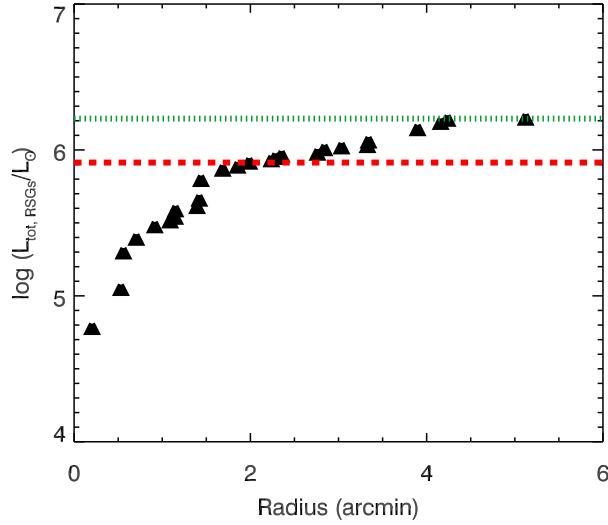


Fig. 14.—: Cumulative luminosity of the cluster, assuming the mean of the star positions to be the cluster centre. The maximum light and half-light are marked with dotted and dashed lines respectively.

**Density parameter, $\eta$:** As we do not have extensive data on many stars in the cluster (the RSGs are the only stars of which we can be sure are cluster members), measuring the $\eta$-parameter is beyond the scope of this work. For now, we use the canonical value of 10, which was shown be Spitzer (1987) to be valid for a range of models.

Using these values and their associated uncertainties, we find a dynamical cluster mass for RSGC2 of $(6\pm4)\times10^4(\eta/10)M_\odot$, assuming the kinematic cluster distance of 5.83kpc. Below, we will compare this value to that found from comparison with theoretical isochrones.

### 4.1.2. Evolutionary models

Following the Monte-Carlo method of FMR06, we generate a coeval cluster of stars with a predefined total cluster mass, and with initial stellar masses drawn randomly from a sample consistent with a Salpeter initial mass-function (IMF) (Salpeter 1955). For a given cluster age, we use the synthetic isochrones created from Geneva non-rotating stellar evolutionary tracks and determine the present-day luminosities and temperatures of the stars in the cluster. We isolate the supergiants as those stars with $\log(L_\star/L_\odot) > 4.0$, and define the red, yellow and blue supergiants as those with temperatures ($T_{\rm eff} < 4500$K), ($4500$K $< T_{\rm eff} < 9000$K), and ($T_{\rm eff} > 9000$)K respectively. We then count the numbers of RSGs for each simulated cluster for a given age and initial mass. Each simulation is repeated $10^3$ times to reduce statistical error. We note that while the statistical uncertainty in the mean number of RSGs per model cluster is negligible, the $1\sigma$ standard deviation of the mean is around 20% (FMR06). Hence cluster parameters which result in $N_{\rm RSG} = 26$ can produce $20\lesssim N_{\rm RSG} \lesssim 32$ for a given trial.

In Fig. 15 we plot the number of RSGs in a coeval cluster of a given initial mass as a function of age. For this plot we use the isochrones with solar metallicity and canonical mass-loss rates of Schaerer et al. (1993). At ages below $\sim$7Myr, very few RSGs are present. The massive stars which have evolved off the MS experience high mass-loss in the BSG phase which prevents their evolution to the red. RSGs begin to appear when those stars with $M_{initial} \sim 25M_\odot$ finish core-hydrogen burning. The number of RSGs then falls off rapidly above $\sim$14Myr as the stars massive enough to become RSGs exhaust their nuclear fuel. Hence, the likelyhood of observing a cluster of 26 RSGs is much higher for cluster ages in the range 7-13Myr.

Figure 15 illustrates that for coeval clusters, only those with $M_{initial} \sim 4 \times 10^4 M_\odot$ can produce numbers of RSGs in excess of 26, the number we observe in this cluster, for the evolutionary models used in Fig. 15. In Fig. 16 we investigate the effect of using isochrones
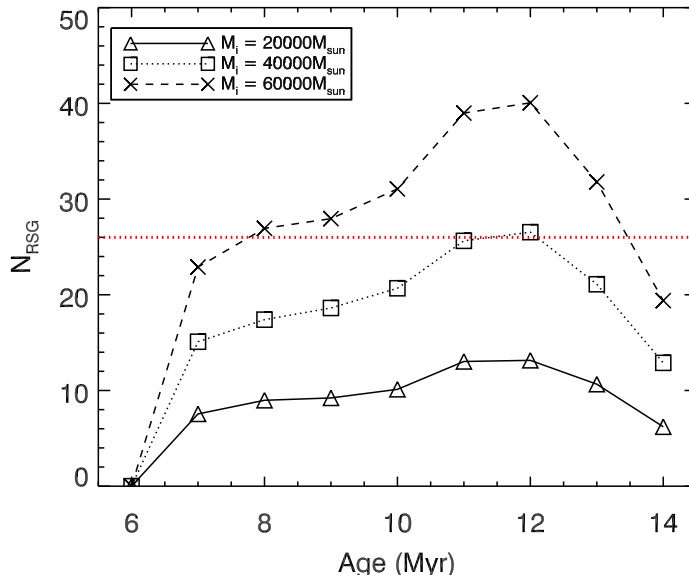
**Fig. 15.**—: The number of RSGs in a cluster as a function of age for three different initial cluster masses, as calculated from the non-rotating Geneva models of Schaerer et al. (1993). The observed number of 26 RSGs is indicated by the red dotted line.

generated with different evolutionary tracks. We plot the results of using isochrones with solar metallicity and canonical mass-loss rates (as used in Fig. 15), solar metallicity with doubled mass-loss rates (Meynet et al. 1994), and twice-solar metallicity. Whilst the different models produce slightly different results, in the likely range of cluster ages of 7-13Myr the model differences are smaller than the statistical variations of individual simulations. We therefore consider this to be a negligible source of uncertainty in this estimate of the cluster mass.

Much progress has been made in recent years in incorporating rotation in stellar structure codes (see review of Maeder & Meynet 2000), so a discussion of the effects of including rotation on our analysis seems warranted. Heger & Langer (2000), Meynet & Maeder (2000), and Heger et al. (2000) studied specifically the effect of rotation on stars in the initial mass range relevant to this work, i.e. $M_\star \sim 15\text{-}25 M_\odot$. The broad result was that rotationally-enhanced mixing increases the chemical homogeneity of the star, leading to larger helium cores, higher luminosities ($\Delta \sim 0.25$dex) and lower effective temperatures ($\Delta \sim 400$K) of RSGs. In addition, stars spent longer on the main-sequence ($\sim 12\%$), due to the decreased effective gravity causing the star behave as a non-rotating star with lower initial mass.

In Fig. 17 we investigate the effect of using the contemporary Geneva models which include stellar rotation. The rotational-velocity grids of these models are, as yet, not complete.
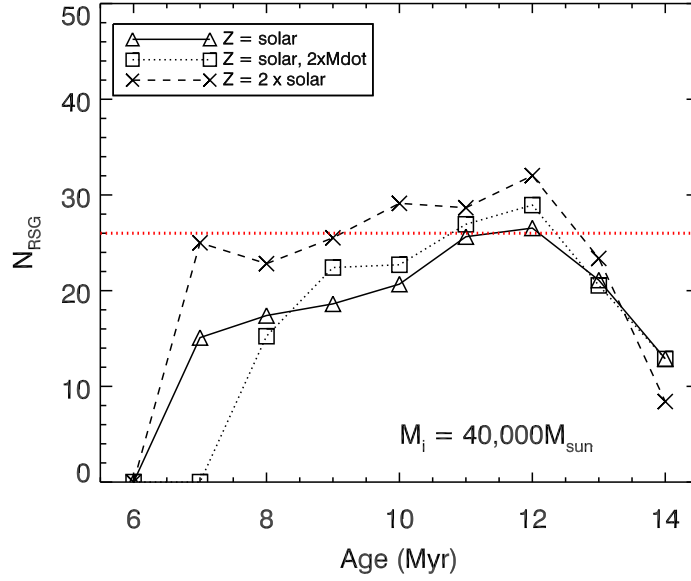
Fig. 16.—: The number of RSGs in a cluster as a function of age for an initial cluster mass of $M_{initial} = 4 \times 10^4 M_\odot$, as calculated from the non-rotating models of Schaerer et al. (1993) and Meynet et al. (1994). Three different evolutionary tracks are investigated: solar metallicity with canonical mass-loss rates; solar metallicity with doubled mass-loss rates; and twice-solar metallicity. The observed number of 26 RSGs is indicated by the red dotted line.
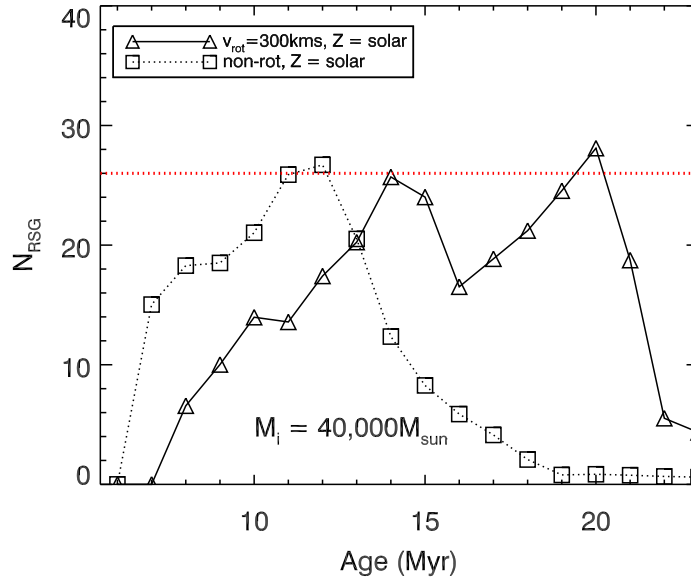


Fig. 17.—: Same as Fig. 16, comparing the non-rotating – solar-metallicity models of Schaerer et al. (1993) with the fast-rotating, solar-metallicity models of Meynet & Maeder (2000).

Here we use the $v_i$=300 km s$^{-1}$ models, which are likely too large for this mass-range and metallicity. However they serve to investigate the impact of stellar rotation on our analysis. As the impact of rotation is greatest on the evolution of massive stars, due to its effect on the mass-loss behaviour, Geneva models are only computed down to $9M_\odot$. To construct isochrones we spline together the massive, rotating models with the non-rotating models of mass $<9M_\odot$.

The Figure shows that, in the early part of the diagram ($\lesssim$15 Myr), the rotating models lag the non-rotating models, due to the longer time spent on the main-sequence. At later times, the rotating models continue to produce RSGs long after the non-rotating models. This can be understood as a combination of longer lifetimes, and the stars' increased luminosity and decreased $T_{\rm eff}$, enabling them to spend longer in the RSG 'zone', as defined by our somewhat arbitrary thresholds of $\log(L/L_\odot) \geq 4.0$ and $T_{\rm eff} \leq 4500$ K. The inclusion of rotation does not affect the inferred lower limit to the initial cluster mass of $M_{initial} \sim 4 \times 10^4 M_\odot$.

From isochrone fitting (see next section), we are able to constrain the age of the cluster to $12 \pm 1$ Myr (non-rotating models) and $17 \pm 3$ Myr (fast-rotating models). From these results, we estimate an 'evolutionary' cluster mass for RSGC2 of $M_{\rm ev} = (4 \pm 1) \times 10^4 M_\odot$. The uncertainty takes into account the statistical variations of the Monte-Carlo method, and the error in the cluster age. The estimate compares well to the dynamical mass of $M_{\rm dyn} = (6\pm4)\times10^4(\eta/10)M_\odot$.

### 4.1.3. The effect of cluster non-coevality

The mass derived above assumes that the stars were created in a coeval starburst. The large extent of the association ($\sim$10pc at a distance of 5.83kpc), as well as the large luminosity spread (see Sect. 4.2), may suggest a sustained starburst phase of several million years. While the large size may be explained by expansion due to non-virial equilibrium (Bastian & Goodwin 2006, see Sect. 4.1.1), and the luminosity spread due to short-comings in evolutionary models (Massey & Olsen 2003, Sect. 4.2), we nonetheless discuss the effect of non-coeval star-formation on our derived total mass.

The effect of cluster non-coevality would be to convolve the curves shown in Fig. 15 with a smoothing function characterized by the length of the starburst phase. Thus, as long as the starburst occured on timescales much shorter than the mean age of the cluster, it would not significantly affect the number of RSGs observed at any one time. For an extended starburst phase of order the inferred age of the cluster, the number of RSGs at any one time for a given cluster mass would decrease. Hence, a prolonged starburst would imply

a larger cluster mass than derived here. The presence of main-sequence O stars or WRs, which have lifetimes of $\sim$3Myr, or low-mass AGB stars with lifetimes of $\gg$20Myr, would imply a sustained star-forming episode. Observations of such stars would require precise radial velocity measurements, such as those presented here, to confirm that they were part of the physical association.

## 4.2. Cluster age

A novel method for estimating the age of a cluster from the RSG population was presented in FMR06. They showed that, using the non-rotating Geneva models, the luminosity range of RSGs for a coeval cluster changes with age (see their Fig. 19). For young ($\lesssim$7Myr) clusters, the RSGs result from stars which have evolved horizontally across the HR diagram, meaning that the RSGs occupy a very narrow luminosity range. For older clusters however, the RSGs – which result from stars of lower initial mass – have a larger luminosity spread, due to the upturn at the end of the evolutionary path (see Fig. 18).
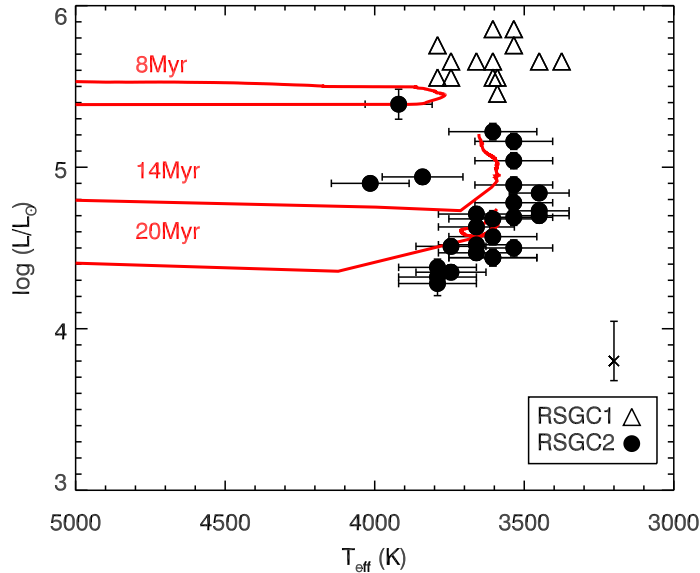


**Fig. 18.**—: H-R diagram, showing the positions of the stars in the two Scutum RSG clusters. Also shown are isochrone fits for each cluster, based on rotating Geneva models with solar metallicity, canonical mass-loss rates, and initial rotational velocity of $300\,\mathrm{km\ s^{-1}}$. As the RSGC2 stars are all at the same distance, the uncertainties shown in $L_{\mathrm{Bol}}$ for these stars do not include the error in the cluster distance. The magnitude of the distance error is indicated seperately in the bottom-right of the panel.

The RSGC2 stars have luminosities ranging from $\log(L/L_\odot) = 4.2 \to 5.2$ (see Table 2). This compares to the larger luminosities and narrower spread of RSGC1, which has $\log(L/L_\odot) = 5.0 \to 5.6$. This can be seen clearly in Fig. 18, which shows the locations of the stars in the two clusters on a H-R diagram. The luminosities of the stars in RSGC1 are taken from FMR06, and have been corrected for the slightly greater distance determined from SiO maser emission by Nakashima & Deguchi (2006) and the contemporary Galactic rotation curve (see above). Isochrone fits to the data, again using the fast-rotating Geneva models of Meynet & Maeder (2000), illustrate the clear age-difference of the clusters. An age of $17 \pm 3$ Myr is consistent for RSGC2, compared to $8 \pm 1$ Myr for RSGC1. When non-rotating isochrones are used, the inferred age of RSGC2 becomes $12 \pm 1$ Myr, while the age of RSGC1 is unchanged. The figure shows that, while there may be some overlap in the absolute uncertainties, there is a clear age-gap between the two clusters of several Myr.

While it is remarkable how the RSGC2 stars tightly follow the 'hockey-stick' end to the isochrone, no single isochrone reproduces the luminosity spread of the stars, with the 20Myr rotating isochrone not extending to the greatest luminosities observed in the cluster. Taking Fig. 18 at face-value, this could imply that the cluster is non-coeval, and formed over a period of 6Myr. However, it was a well-known problem that the non-rotating evolutionary models did not reproduce the highest observed luminosities of RSGs (Massey & Olsen 2003); and while the inclusion of rotation in evolutionary codes does in general make RSGs redder and brighter, it is not clear that the difference between observation and expectation has been completely reconciled. Indeed, the RSGCs may be the ideal laboratory in which to test these models.

## 4.3. Unidentified objects near RSGC2: evidence of recent starburst activity at the base of the Scutum-Crux arm.

From the derived distances to the two RSG clusters, their separation is of order 100pc. The proximity of these two remarkable objects to one another, combined with their similar ages, is perhaps indicative of a wider-scale starburst episode in the region of the Scutum-Crux spiral arm. As noted by Nakashima & Deguchi (2006), the inferred distances for the objects put them close to where the spiral arms meet the Galactic bulge, roughly the co-rotation radius of the bulge bar (Bissantz et al. 2003), and in the middle of the proposed high-density 'stellar ring' (Bertelli et al. 1995). The physical conditions and gas dynamics in this region of the Galaxy may precipitate star formation activity, while the location of the clusters within one of the co-rotation Lagrangian points (Englmaier & Gerhard 1999) may harbour the clusters from tidal disruption.
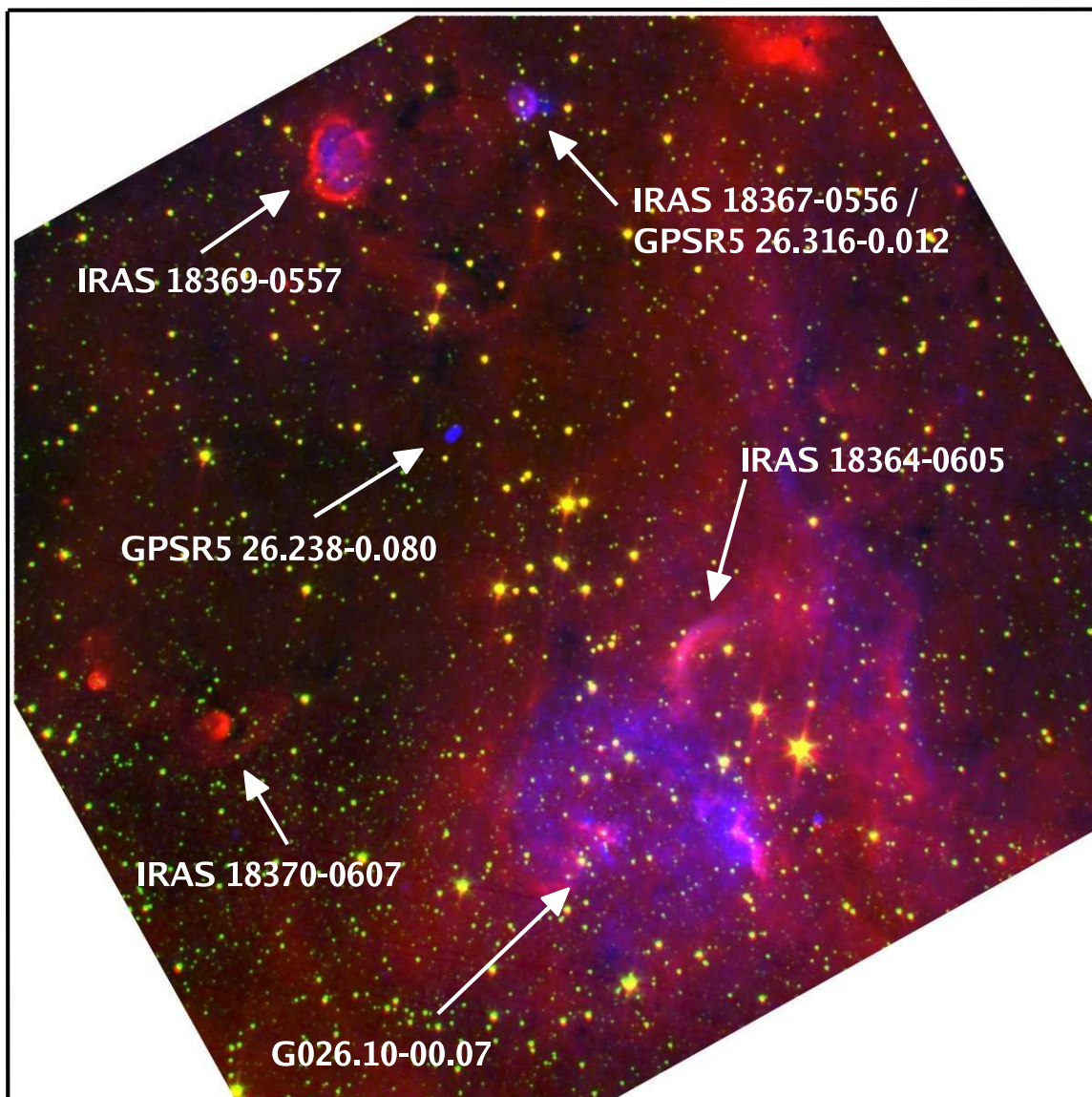
Fig. 19.—: RGB-composite image of the region around RSGC2. The image shows the *Spitzer/GLIMPSE* bands 8.0μm (red), 4.5μm(green), and *MAGPIS*-20cm (blue). Sources identified in radio surveys, as well as the likely origin of several *IRAS* point-sources, are marked on the image.

As we are looking tangentially along the Galactic arm at the point where it meets the bulge, it is reasonable to assume that there may be other evidence of recent star-formation along our line-of-sight towards the two clusters. Indeed, separate from the cluster stars, there appear to be further RSGs in the direction of RSGC2. These objects have CO equivalent widths too large to be giants, but their radial velocities are inconsistent with being part of the cluster itself. These stars may be part of smaller clusters formed in a region-wide starburst phase around $\sim$10–20Myrs ago.

FMR06 discussed the possibility that various unidentified high-energy/radio sources in the region of RSGC1 were due to recent supernova activity, although the nonthermal radio-sources have since been shown to be extra-galactic (Trejo & Rodríguez 2006). Here, we make a similar discussion of the unidentified sources near RSGC2, using the Galactic plane survey data of *GLIMPSE*, *MIPSGAL* and *MAGPIS* (Benjamin et al. 2003; Carey et al. 2005; Helfand et al. 2006).

Figure 19 shows a composite of *IRAC* channels 2 (4.5$\mu$m) and 4 (8.0$\mu$m), and *VLA*-20cm, centred on RSGC2. The image shows in detail for the first time several radio and *IRAS* point-sources, as well as the HII-region G26.10-0.07. Below, we discuss the nature of each of these objects, as well as their relation to RSGC2 and the starburst phase in which it was created.

**IRAS 18369-0557**  When seen in detail (see images in Fig. 20), this object has the appearance of a discrete ring of material, which seems to peak in the 5.8 & 8$\mu$m bands. Inside this ring is filled-in with 20cm-emission, and the inner material is also bright at 24$\mu$m such that it saturates the *MIPSGAL* image. The object is not detected in *2MASS*, nor is it detected in *IRAC* bands 1 or 2. No obvious central point-source is observed in any band. Aside from the bright ring, there is also a dark arc extending from the SE to the NW. This arc may be due to cold dust, oriented in some polar outflow perpendicular to the bright ring.

That the ring is so bright at 5.8$\mu$m but not seen at 4.5$\mu$m, with the central region peaking at $\sim$24$\mu$m, suggests that the emission may be due to warm ($\sim$100K) dust, with strong PAH emission at 5$\mu$m in the outer ring. Detailed temperature modelling of the dust would benefit from mid-IR spectroscopy across the nebula, such a study is beyond the scope of the current work.

From the object's appearance and the apparent lack of any central source, it is tempting to classify the object as a supernova remnant (SNR). The semi-major axis of the ring is 1.5$'$ across, which at the distance of RSGC2 corresponds to a diameter of 2.5pc. If we assume a typical SN expansion speed of $\sim$1000 km s$^{-1}$, this would make the remnant $\sim$2500 years old
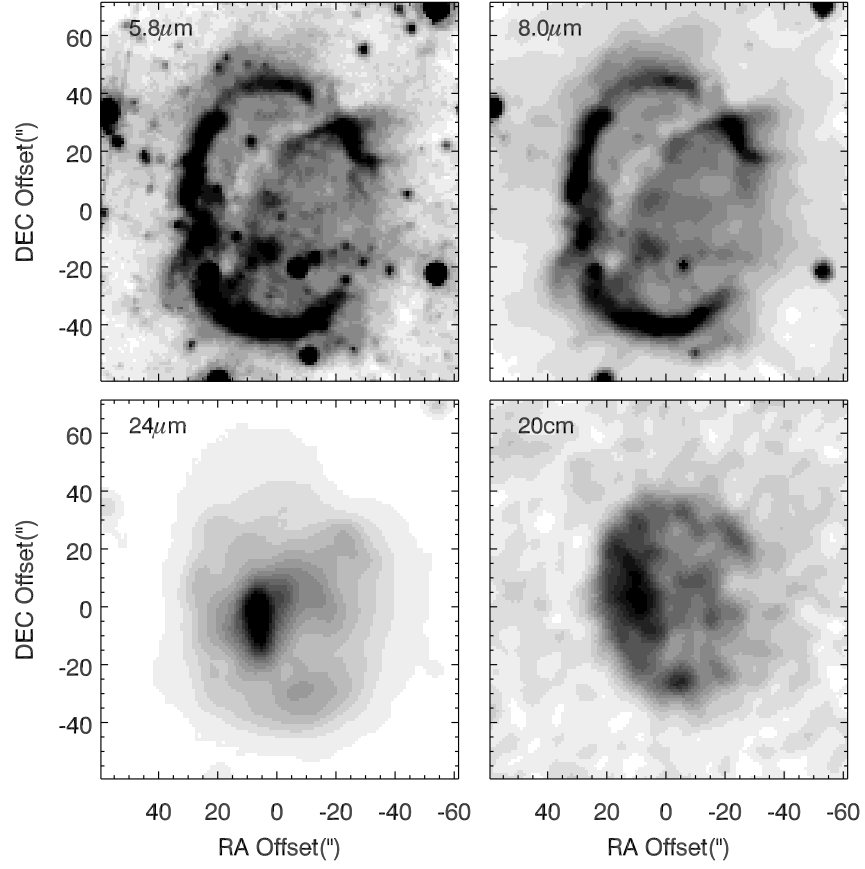
**Fig. 20.**—: High-resolution images of the IRAS 18369-0557 source. Top-left: Spitzer/IRAC 5.8$\mu$m; top-right: Spitzer/IRAC 8.0$\mu$m; bottom-left: MIPS 24$\mu$m; bottom-right: VLA 20cm. All images are scaled linearly between 0-7$\sigma$ above the sky background.
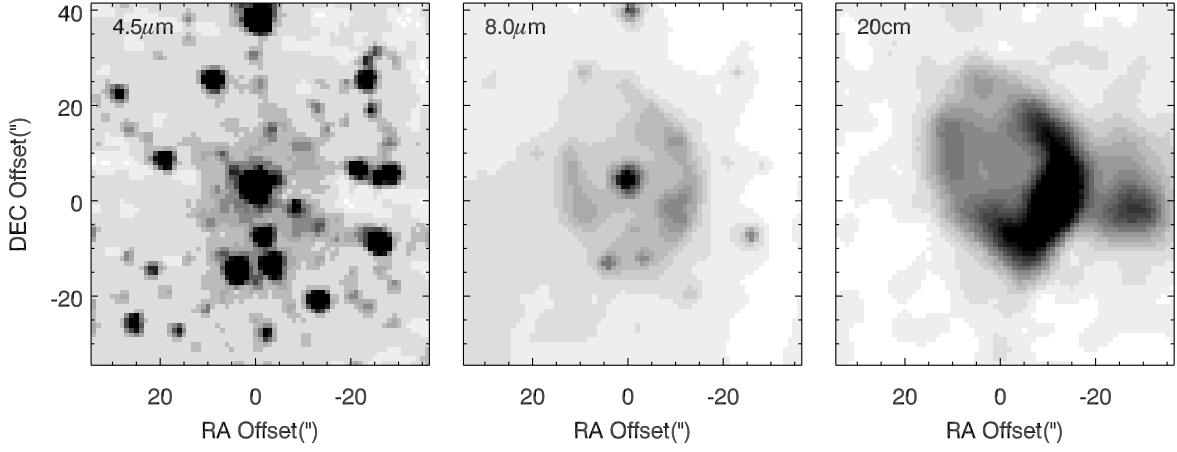
**Fig. 21.—:** High-resolution images of the IRAS 18367-0556 source. Left: Spitzer/IRAC 4.5$\mu$m; centre: Spitzer/IRAC 8.0$\mu$m; right: VLA 20cm. All images are scaled linearly between 0-10$\sigma$ above the sky background.

*if* the dust has formed out of the SN ejecta. It would seem unlikely that 100K dust would survive this long; by comparison, Blair et al. (2007) find that Kepler's SNR, which is ∼4kpc away and ∼400 years old, is already very faint at 5.8$\mu$m. A more likely explanation is that the dust was produced in a pre-SN mass-losing phase of the precursor, and has been heated by the SN explosion which must have occured less than a few hundred years ago. Such a situation is seen to be happening in SN 1987A (Bouchet et al. 2006).

It was argued in FMR06, using evolutionary models, that a cluster similar to RSGC1 should experience SNe explosions every ∼40,000-80,000 yr. For RSGC2, which appears to be 50% more massive but a little older, the corresponding timscale is around 50,000yrs. If a SN remnant takes around $10^4$ yrs before it becomes too faint to observe, then it is not unreasonable to assume that we may observe one recent supernova in a cluster like RSGC2. We note that at present there is currently no associated high-energy source, and so classification of the object would benefit from X-ray / $\gamma$-ray observations.

**IRAS 18367-0556 / GPRS5 26.316-0.012**   This object is another radio-bright, 8$\mu$m-bright ring-nebula, this time with a highly-reddened star at the centre ($H - K_S$=1.7). The GLIMPSE and MAGPIS images of the object are shown in Fig. 21. It is so bright at 24$\mu$m that it saturates the corresponding *MIPSGAL* image. The object is reminiscent of an evolved star surrounded by the ejecta of a previous high mass-losing phase, such as a post-AGB star, an LBV, or a WR star. Indeed, it is reminiscent of the mid-IR ring-nebulae seen around

candidate LBVs in the *MSX* survey (Clark et al. 2003), in particular G26.47+0.02.

The radio source is detected in the 1.4GHz NRAO VLA Sky Survey (NVSS) (Condon et al. 1998), and has a flux of 65.6±2 mJy. However, the source is flagged in the survey as being 'complex', possibly due to the size of the source ($\sim$40$''$) being comparable to the size of the beam (FWHM=45$''$). From Fig. 21 it appears that the bulk of the radio emission is coincident with the south-western part of the dust-ring, rather than with the central star. It is therefore unlikely that the radio emission results from the ionized stellar wind, as one would expect to see emission from the base of the wind coincident with the central star. The radio emission could be explained by a hot central star ionizing the surrounding ejecta, or the fast wind of a hot phase ploughing into a slower, dusty wind ejected when the star was cooler.

The object is very reminiscent of the LBV candidate HD 168625 (Robberto & Herbst 1998), speculated by Smith (2007) to be a Galactic analogue of the progenitor of SN 1987A based on the recent discovery of an 8$\mu$m ring around the star. Clearly, further study of IRAS 18367-0556 is warranted, in particular near-IR spectroscopy to determine the stellar temperature, compare the star's radial velocity with the nearby RSG cluster, and to potentially determine abundances of Fe and $\alpha$-group elements in this region of the Galaxy (see e.g. Introduction of Najarro et al. 2004).

**GPSR5 26.238-0.080**   This is an extremely compact radio source, with no obvious counterpart in *2MASS*, *GLIMPSE*, or *MIPSGAL*. For this reason, we suspect this source may be extra-galactic.

**IRAS 18370-0607**   From the *GLIMPSE*-8$\mu$m image, this object and the object just to the north-east appear to be either post-merger galaxies, or pinwheel nebulae as seen in interacting binary systems. That there are two such objects close together seems to favour the former explanation, although the extinction through this region of the Galaxy would mean that these objects were extremely intrinsically bright. For now we draw no definite conclusions as to the nature of these objects.

**G026.10-00.07**   This source was observed in the radio survey of Downes et al. (1980), who measured radial velocities of 33 km s$^{-1}$ from H110$\alpha$ and 104 km s$^{-1}$ from H$_2$CO. It would seem likely that the object as seen in Fig. 19 is a foreground HII-region, and the H$_2$CO beam was contaminated by emission from the RSGs.

Wink et al. (1982) determine that for near- and far-side kinematic distances of the object, using the velocity measured by Downes et al. (1980), the rate of Lyman continuum photons absorbed is $\log(N_{\mathrm{Ly}}/s) = 48.54/50.08$. As the far-side distance would imply an extraordinarily-massive cluster of $\sim$8 O3 stars (e.g. Sternberg et al. 2003), and as no obvious central cluster is seen, the nearside distance seems more likely.

**Star 1, Star 49, and IRAS 18364-0605**   It can be seen from Fig. 22 that Star 49 has remarkable near- and mid-IR excess. In addition, the IRAC images show the star apparently at the centre-of-curvature of a bow-shock structure, identified in the *IRAS* point-source catalogue as IRAS 18364-0605. Star 49 itself is one of the most luminous stars in the cluster, while having an earlier-than-average spectral-type (K3). The star's temperature places it close to the Yellow Hypergiants, a short evolutionary phase experienced by stars on their way from the RSG to the LBV/WR stages (de Jager 1998). In clusters containing so many RSGs, it is not unreasonable to expect to find one such object (see also Star 15 in RSGC1, FMR06).

Star 49 is not as hot as the YHGs, however the large IR-excess is suggestive of large amounts of warm circumstellar dust ejected in a high mass-losing episode, possibly a pre-cursor to blue-ward evolution. It would be interesting to measure the mass-loss rate of this object, and compare it to that of outburst of the YHG IRC +10 420, during which the mass-loss rate is inferred to have reached $5\times10^{-4}M_{\odot}\mathrm{yr}^{-1}$ (Oudmaijer et al. 1996). Since evolved then the star has apparently evolved to an A-type supergiant (Klochkova et al. 2002), though this may be due to the dissipation of the pseudo-photosphere created by the dense wind (Smith et al. 2004).

Star 1 is by far the brightest object in this field in the $K$-band ($K_S$=2.9), and is highly reddened ($H - K_S$=1.798). It is not possible to fit this star with a standard reddening law, assuming the late spectral type of M5-6 derived from its CO-bandhead absorption. It is likely this object has significant IR excess, possibly due to an extreme mass-losing episode. Its radial velocity is $\sim$20 km s$^{-1}$ below that of the rest of the 'cluster' stars, hence it is unlikely to be a foreground giant. Indeed, the star may be part of the RSGC2 cluster, and its observed radial velocity offset by an expanding optically-thick envelope; the velocity difference of $\sim$20 km s$^{-1}$ is a typical outflow-speed for a RSG. It is possible that this star is an extreme Red Hypergiant, such VY CMa – a star with large IR excess and inferred mass-loss rate of $\sim$2$\times10^{-4}M_{\odot}$ (Danchi et al. 1994).

The Red- and Yellow-Hypergiants are extremely rare objects, however it is not clear whether this is due to the exceptional nature of certain stars, or whether all stars of a particular initial mass-range and metallicity will pass through brief but extreme mass-losing

episodes such as these. If the latter is true, it is then not unreasonable to expect to find such stars among the two Scutum-Crux RSG clusters, as RSGC1 & 2 appear to be of just the right age and initial mass. Stars 1 and 49 certainly warrant further study in the context of the evolution of RSGs at Galactic metallicity, as they appear to be on the verge of shedding their outer layers and evolving blueward toward the LBV/WN phases.

## 4.4. The RSG clusters in the broader context of astrophysics

From the cluster mass and age derived here, RSGC2 joins the nearby RSGC1 (FMR06), Westerlund 1 (Wd 1, Clark et al. 2005), the Arches (Figer et al. 2002), Quintuplet (Figer et al. 1999), and Galactic centre (GC, Figer et al. 2004) clusters, in a growing list of Galactic analogues to Super Star Clusters. These objects represent ideal natural laboratories in which to study the evolution of massive stars. The Arches cluster is massive enough and young enough to contain main-sequence O-stars up to the mass of $\sim 150 M_\odot$ (Figer et al. 2002), whilst the age and mass of Wd 1 is tuned in such a way that it contains 24 WRs – 8% of all those known in the Galaxy (Clark & Negueruela 2002; Negueruela & Clark 2005; Groh et al. 2006; Crowther et al. 2006). Meanwhile Martins et al. (2007) recently applied abundance analysis to the unusually-large number of Opfe/WN9 stars in the GC cluster to tie down their evolutionary status.

Of this collection of massive Galactic clusters, the two RSG clusters are evidently the elder, not only from the population-synthesis analysis presented here and in FMR06, but also from the lack of diffuse radio emission at the centre of the clusters, and hence of few remaining hot main-sequence stars (we note that, while RSGC2 has a radio nebula just to the south-west, radio recombination line observations place this object in the foreground – see Sect. 4.3).

This gives the two clusters a unique role in the context of massive stellar evolution, as they offer the opportunity to study a statistically-significant population of RSGs and probe the evolution of stars in the mass-range of $\sim 15\text{-}25 M_\odot$. Evidence is growing that such stars are the progenitors of Type-II SNe (Van Dyk et al. 2003; Smartt et al. 2004), while they may contribute significantly toward Galactic-scale dust production, particularly in low-metallcity starbursts where Carbon-sequence WRs are absent and AGB stars are yet to form (see discussion by Massey et al. 2005).

As hinted by the distribution of spectral-types (Sect. 3.3), the clusters likely have similar abundances, representative of the rest of the Galaxy. In addition, the fact that there are *two* clusters, with slightly different ages – and hence initial masses of RSGs – now permits

evolutionary studies at uniform metallicity, and as a function of initial mass.

### 4.4.1. The RSGCs as a probe of the Galactic Z-gradient

Aside from the unusually-large number of RSGs and the opportunities they present for studying stellar evolution, an additional interesting aspect of the clusters is their location in the Galactic plane at a Galacto-centric distance of ∼4kpc. Here, they are close to where the disk meets the central bulge, within the proposed 'ring' of enhanced stellar density (Bertelli et al. 1995).

Chemical abundance analyses of this region could be key to understanding the formation and evolution of our Galaxy, in the transition zone between the Galactic disk and bulge. An important constraint on models of the formation of the Galaxy and its central bulge is the radial metallicity gradient. Abundance analyses of HII regions, planetary nebulae, and early-type stars have found a steadily increasing metal content from $18 - 5$kpc (e.g. Afflerbach et al. 1997; Maciel & Quireza 1999; Rolleston et al. 2000). The metallicity within 5kpc of the Galactic centre is less clear: Smartt et al. (2001) find that the metallicity continues to increase at the same slope down to 2.5kpc, although curiously not for oxygen; while studies of the inner ∼50pc have have revealed roughly solar abundances (e.g. Ramírez et al. 2000; Najarro et al. 2004).

The RSGCs are now a powerful tool with which to probe what could potentially be the transition zone between the Galactic disk and bulge, and the location where the metallicity gradient breaks down. Near-IR spectral analyses of RSGs can yield Fe abundances (e.g. Rich & Origlia 2005); while analysis of the LBV candidate, and any BSGs in the clusters, would provide direct measurements of Fe and $\alpha$-group elements such as Si and Mg (Najarro 2006).

## 5. Conclusions

Using near-IR spectroscopy, and 2MASS/GLIMPSE/MSX photometry, we have shown that there is a second reddened, massive young cluster of RSGs in the Galactic plane at $l = 25 - 26°$. We find that this cluster, RSGC2, contains 26 RSGs, almost twice as many as the nearby RSGC1. From evolutionary synthesis and kinematic measurements we infer that RSGC2 is slightly older and the more massive of the two, with a mass comparable to that of Westerlund 1. Together, the two Scutum-Crux RSG clusters harbour ∼20% of all known RSGs in the Galaxy, and now offer an unprecedented opportunity to study pre-

supernova evolution at uniform metallicity. Further, new infrared/radio survey images reveal several background RSGs, and candidates for a supernova remnant and a Luminous Blue Variable in the field of RSGC2. Along with the proximity of RSGC1, this suggests intense, recent, region-wide star-formation activity at the point where the Scutum-Crux Galactic arm meets the Galactic bulge. Future abundance studies of this region would yield important information in the study of the Galactic metallicity gradient, and the interaction between the disk and the bulge.

## REFERENCES

Afflerbach, A., Churchwell, E., & Werner, M. W. 1997, ApJ, 478, 190

Bastian, N. & Goodwin, S. P. 2006, MNRAS, 369, L9

Benjamin, R. A., Churchwell, E., Babler, B. L., et al. 2003, PASP, 115, 953

Bertelli, G., Bressan, A., Chiosi, C., Ng, Y. K., & Ortolani, S. 1995, A&A, 301, 381

Bica, E., Dutra, C. M., & Barbuy, B. 2003a, A&A, 397, 177

Bica, E., Dutra, C. M., Soares, J., & Barbuy, B. 2003b, A&A, 404, 223

Bissantz, N., Englmaier, P., & Gerhard, O. 2003, MNRAS, 340, 949

Blair, W. P., Ghavamian, P., Long, K. S., et al. 2007, ApJ, 662, 998

Bouchet, P., Dwek, E., Danziger, J., et al. 2006, ApJ, 650, 212

Buchanan, C. L., Kastner, J. H., Forrest, W. J., et al. 2006, AJ, 132, 1890

Carey, S. J., Noriega-Crespo, A., Price, S. D., et al. 2005, in Bulletin of the American Astronomical Society, 1252–+

Caron, G., Moffat, A. F. J., St-Louis, N., Wade, G. A., & Lester, J. B. 2003, AJ, 126, 1415

Clark, J. S., Egan, M. P., Crowther, P. A., et al. 2003, A&A, 412, 185

Clark, J. S. & Negueruela, I. 2002, A&A, 396, L25

Clark, J. S., Negueruela, I., Crowther, P. A., & Goodwin, S. P. 2005, A&A, 434, 949

Condon, J. J., Cotton, W. D., Greisen, E. W., et al. 1998, AJ, 115, 1693

Crowther, P. A., Hadfield, L. J., Clark, J. S., Negueruela, I., & Vacca, W. D. 2006, MNRAS, 372, 1407

Cutri, R. M., Skrutskie, M. F., van Dyk, S., et al. 2003, 2MASS All Sky Catalog of point sources. (The IRSA 2MASS All-Sky Point Source Catalog, NASA/IPAC Infrared Science Archive. http://irsa.ipac.caltech.edu/applications/Gator/)

Danchi, W. C., Bester, M., Degiacomi, C. G., Greenhill, L. J., & Townes, C. H. 1994, AJ, 107, 1469

de Jager, C. 1998, A&A Rev., 8, 145

Downes, D., Wilson, T. L., Bieging, J., & Wink, J. 1980, A&AS, 40, 379

Dutra, C. M., Bica, E., Soares, J., & Barbuy, B. 2003, A&A, 400, 533

Egan, M. P., Price, S. D., & Gugliotti, G. M. 2001, in Bulletin of the American Astronomical Society, 561–+

Eisenhauer, F., Genzel, R., Alexander, T., et al. 2005, ApJ, 628, 246

Elias, J. H., Frogel, J. A., & Humphreys, R. M. 1985, ApJS, 57, 91

Englmaier, P. & Gerhard, O. 1999, MNRAS, 304, 512

Feast, M. & Whitelock, P. 1997, MNRAS, 291, 683

Figer, D. F., Gilmore, D., Kim, S. S., et al. 2003, ApJ, 599, 1139

Figer, D. F., MacKenty, J. W., Robberto, M., et al. 2006, ApJ, 643, 1166

Figer, D. F., McLean, I. S., & Morris, M. 1999, ApJ, 514, 202

Figer, D. F., Najarro, F., Gilmore, D., et al. 2002, ApJ, 581, 258

Figer, D. F., Rich, R. M., Kim, S. S., Morris, M., & Serabyn, E. 2004, ApJ, 601, 319

Fluks, M. A., Plez, B., The, P. S., et al. 1994, A&AS, 105, 311

Groh, J. H., Damineli, A., Teodoro, M., & Barbosa, C. L. 2006, A&A, 457, 591

Heger, A., Fryer, C. L., Woosley, S. E., Langer, N., & Hartmann, D. H. 2003, ApJ, 591, 288

Heger, A. & Langer, N. 2000, ApJ, 544, 1016

Heger, A., Langer, N., & Woosley, S. E. 2000, ApJ, 528, 368

Helfand, D. J., Becker, R. H., White, R. L., Fallon, A., & Tuttle, S. 2006, AJ, 131, 2525

Humphreys, R. M. 1979, ApJ, 231, 384

Indebetouw, R., Mathis, J. S., Babler, B. L., et al. 2005, ApJ, 619, 931

Josselin, E., Blommaert, J. A. D. L., Groenewegen, M. A. T., Omont, A., & Li, F. L. 2000, A&A, 357, 225

Kleinmann, S. G. & Hall, D. N. B. 1986, ApJS, 62, 501

Klochkova, V. G., Yushkin, M. V., Chentsov, E. L., & Panchuk, V. E. 2002, Astronomy Reports, 46, 139

Kothes, R. & Dougherty, S. M. 2007, ArXiv e-prints, 0704.3073

Kudritzki, R.-P. & Puls, J. 2000, ARA&A, 38, 613

Levesque, E. M., Massey, P., Olsen, K. A. G., et al. 2005, ApJ, 628, 973

Maciel, W. J. & Quireza, C. 1999, A&A, 345, 629

MacKenty, J. W., Greenhouse, M. A., Green, R. F., et al. 2003, in Instrument Design and Performance for Optical/Infrared Ground-based Telescopes. Edited by Iye, Masanori; Moorwood, Alan F. M. Proceedings of the SPIE, Volume 4841, pp. 953-961 (2003)., ed. M. Iye & A. F. M. Moorwood, 953–961

Maeder, A. & Meynet, G. 2000, A&A, 361, 159

Martins, F., Genzel, R., Hillier, D. J., et al. 2007, ArXiv Astrophysics e-prints

Massey, P. & Olsen, K. A. G. 2003, AJ, 126, 2867

Massey, P., Plez, B., Levesque, E. M., et al. 2005, ApJ, 634, 1286

Maund, J. R., Smartt, S. J., Kudritzki, R. P., Podsiadlowski, P., & Gilmore, G. F. 2004, Nature, 427, 129

McLean, I. S., Becklin, E. E., Bendiksen, O., et al. 1998, in Proc. SPIE Vol. 3354, p. 566-578, Infrared Astronomical Instrumentation, Albert M. Fowler; Ed., ed. A. M. Fowler, 566–578

Mengel, S., Lehnert, M. D., Thatte, N., & Genzel, R. 2002, A&A, 383, 137

Messineo, M., Habing, H. J., Menten, K. M., et al. 2005, A&A, 435, 575

Meynet, G. & Maeder, A. 2000, A&A, 361, 101

Meynet, G., Maeder, A., Schaller, G., Schaerer, D., & Charbonnel, C. 1994, A&AS, 103, 97

Najarro, F. 2006, Journal of Physics Conference Series, 54, 224

Najarro, F., Figer, D. F., Hillier, D. J., & Kudritzki, R. P. 2004, ApJ, 611, L105

Nakashima, J.-i. & Deguchi, S. 2006, ApJ, 647, L139

Nakaya, H., Watanabe, M., Ando, M., Nagata, T., & Sato, S. 2001, AJ, 122, 876

Negueruela, I. & Clark, J. S. 2005, A&A, 436, 541

Ortolani, S., Bica, E., Barbuy, B., & Momany, Y. 2002, A&A, 390, 931

Oudmaijer, R. D., Groenewegen, M. A. T., Matthews, H. E., Blommaert, J. A. D. L., & Sahu, K. C. 1996, MNRAS, 280, 1062

Ramírez, S. V., Sellgren, K., Carr, J. S., et al. 2000, ApJ, 537, 205

Reid, M. J. & Brunthaler, A. 2004, ApJ, 616, 872

Rich, R. M. & Origlia, L. 2005, ApJ, 634, 1293

Rieke, G. H. & Lebofsky, M. J. 1985, ApJ, 288, 618

Robberto, M. & Herbst, T. M. 1998, ApJ, 498, 400

Rolleston, W. R. J., Smartt, S. J., Dufton, P. L., & Ryans, R. S. I. 2000, A&A, 363, 537

Salpeter, E. E. 1955, ApJ, 121, 161

Schaerer, D., Charbonnel, C., Meynet, G., Maeder, A., & Schaller, G. 1993, A&AS, 102, 339

Smartt, S. J., Maund, J. R., Hendry, M. A., et al. 2004, Science, 303, 499

Smartt, S. J., Venn, K. A., Dufton, P. L., et al. 2001, A&A, 367, 86

Smith, N. 2007, AJ, 133, 1034

Smith, N., Vink, J. S., & de Koter, A. 2004, ApJ, 615, 475

Sonneborn, G., Altner, B., & Kirshner, R. P. 1987, ApJ, 323, L35

Spitzer, L. 1987, Dynamical evolution of globular clusters (Princeton, NJ, Princeton University Press, 1987, 191 p.)

Stephenson, C. B. 1990, AJ, 99, 1867

Sternberg, A., Hoffmann, T. L., & Pauldrach, A. W. A. 2003, ApJ, 599, 1333

Trejo, A. & Rodríguez, L. F. 2006, Revista Mexicana de Astronomia y Astrofisica, 42, 147

Van Dyk, S. D., Li, W., & Filippenko, A. V. 2003, PASP, 115, 1289

van Loon, J. T., Cioni, M.-R. L., Zijlstra, A. A., & Loup, C. 2005, A&A, 438, 273

Wallace, L. & Hinkle, K. 1996a, ApJS, 103, 235

Wallace, L. & Hinkle, K. 1996b, ApJS, 107, 312

Wallace, L. & Hinkle, K. 1997, ApJS, 111, 445

Whitelock, P., Menzies, J., Feast, M., et al. 1994, MNRAS, 267, 711

Wink, J. E., Altenhoff, W. J., & Mezger, P. G. 1982, A&A, 108, 227
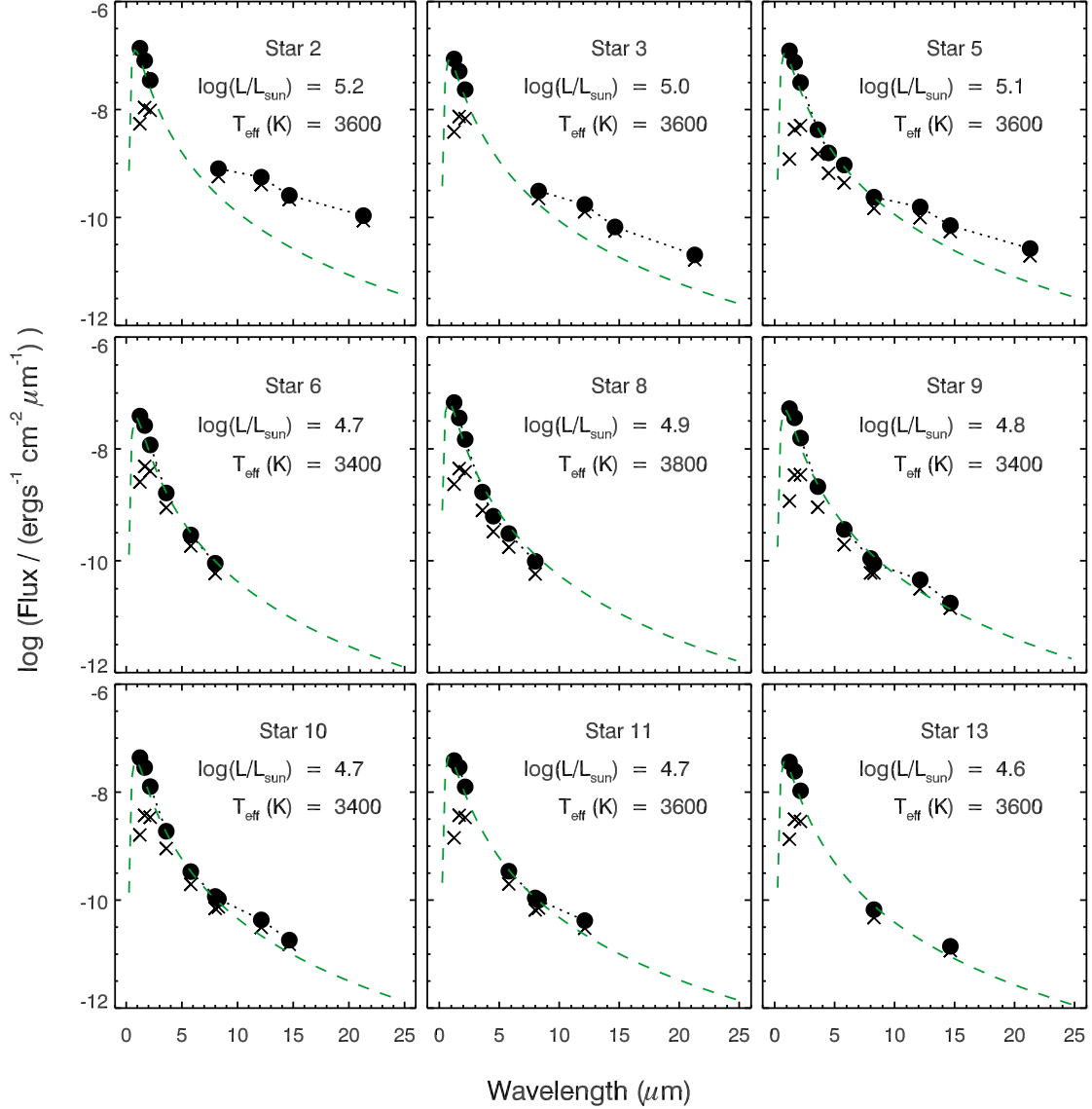
## A.   Appendix

**Fig. 22.**—: Spectral energy distributions of the cluster members, using data from the point-source catalogues of *2MASS*, *GLIMPSE* and *MSX*. The raw photometry is plotted as crosses, and the de-reddened photometry as filled circles. Neither *GLIMPSE* data below 5σ, nor *MSX* upper-limit data are plotted. The green dotted-line in each panel represents a black-body curve appropriate for each star's $K_S$-band magnitude, reddening and temperature, and the kinematic distance to the cluster. We note that there may be some contamination in the *MSX* aperture between Stars 2 and 6, which may explain the large mid-IR excess of Star 2.
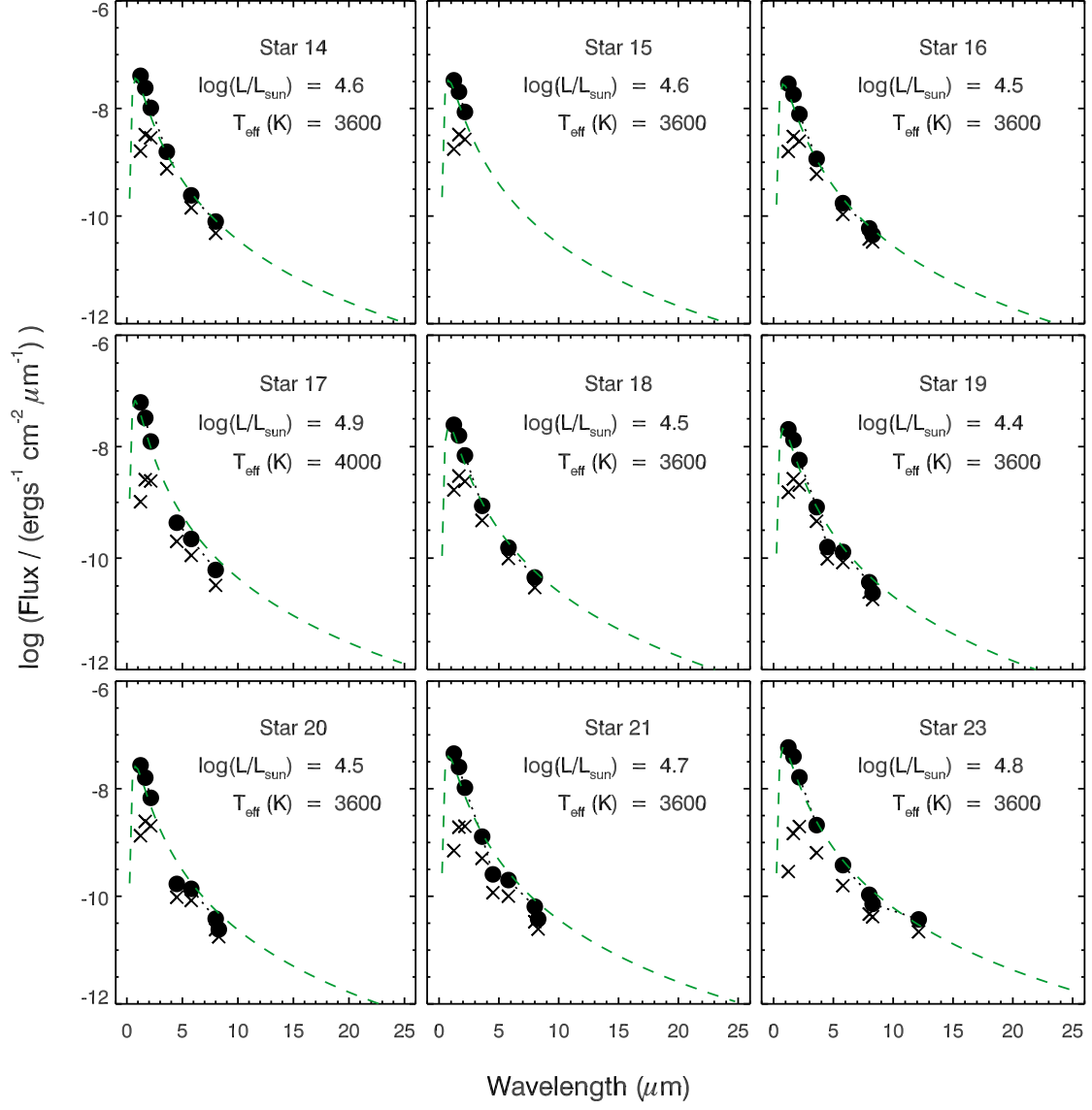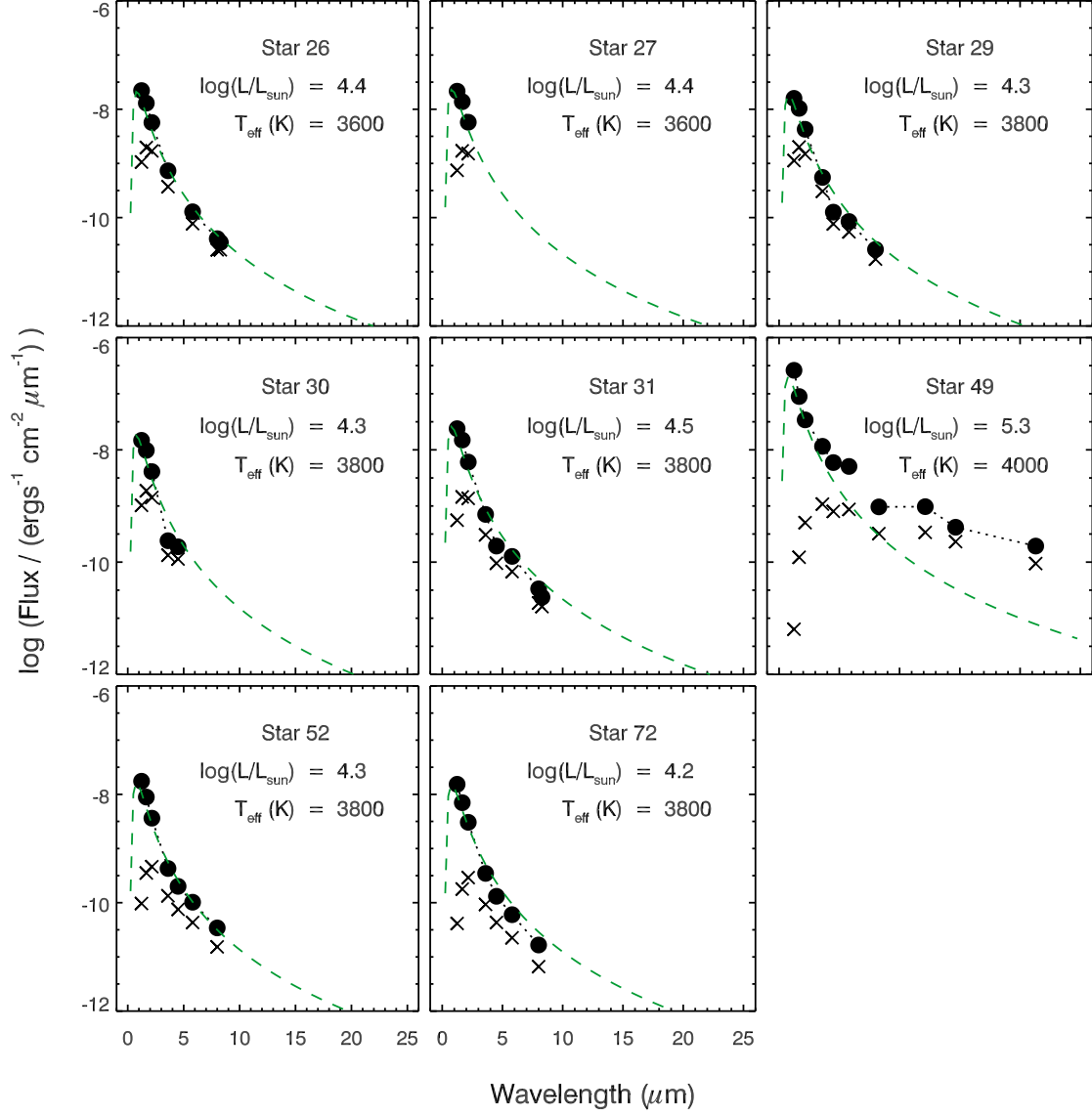
**Fig. 22.**—: cont.

**Fig. 22.**—: cont.